WILEY-VCH

Supporting Information

Pitaya-Inspired Metal-Organic Framework Nanozyme for Multimodal Imaging-Guided Synergistic Cuproptosis, Nanocatalytic Therapy, and Photothermal Therapy

Quer Yue, Qingbin Zeng, Qianni Guo, Xiuchao Zhao, Yaping Yuan, Yuqi Yang, Weiping Jiang, Xin Zhou**

*X. Zhou; Q. Guo

Email: xinzhou@wipm.ac.cn; qian-niguo@wipm.ac.cn

Experiment Section

Materials

Zinc acetate dihydrate ($Zn(OAc)_2·2H_2O$), 30% hydrogen peroxide aqueous solution, 3,3′,5,5′-Tetramethylbenzidine, Rhodamine B, zinc nitrate hexahydrate ($Zn(NO_3)_2·6H_2O$), copper(II) chloride dihydrate ($CuCl_2·2H_2O$), polyvinyl pyrrolidone (PVP, 30 k, Sinopharm, China), sodium sulfide (Na_2S, Lingfeng, China), nitrotetrazolium blue chloride (NBT), L-methionine, riboflavin (Macklin China), 2-methylimidazole (2-MI), indocyanine green (ICG) (Bide China). All chemicals utilized in this study were of analytical grade. Human non-small cell lung cancer cells (A549) were procured from the National Collection of Authenticated Cell Cultures, Shanghai. F12K medium (Boster China), fetal bovine serum (FBS) (Cell-box, Hong Kong), penicillin-streptomycin solution (Biosharp, China). 5,5-dimethyl-1-pyrroline N-oxide (DMPO), 5-tert-butoxycarbonyl-5-methyl-1-pyrroline-N-oxide (BMPO), (Dojindo, Japan), Cell Counting Kit-8 (CCK-8, Labgic, China), Calcein-AM/PI Double Stain Kit (Baiaolaibo,

China), DAPI staining solution, Hoechst 33342 solution, Acridine Orange (AO) Staining Kit, 2′,7′-dichlorofluorescin diacetate (DCFH-DA), ER-Tracker Green, Mito-Tracker Red CMXRos (Beyotime, China), α-ketoglutaric acid (α-KG) content assay kit, pyruvate (PA) content assay kit, FITC Phalloidin (Solarbio, China). Succinate (succinic acid) Assay ELISA Kit (Xinyuan, China). Apoptosis kit with annexin V-FITC and PI (Multisciences, China), Heat Shock Protein 70 (HSP70) antibody, FDX1 antibody, DLAT antibody (ABclonal, China). Deionized water (Millipore) with a resistivity of 18.2 MΩ·cm was utilized in all experiments.

Methods

Characterization

BET surface area and pore size measurements were conducted using N_2 adsorption/desorption isotherms at 77 K on a Micromeritics ASAP 3020 instrument after samples were degassed at 120°C for 12 h. Powder X-ray diffraction (PXRD) patterns were acquired on a Bruker D8 3 kW instrument using Cu Ka radiation (l = 0.15 nm). XPS analysis was performed using a Thermo Fisher 250Xi instrument. TGA-DSC analyses were carried out on a Mettler TG-DSC 3+ instrument under an air atmosphere (test temperature range: 30-800°C, air flow rate: 60 mL min^{-1}). The size and morphology of the materials were analyzed using high-resolution scanning electron microscopy (SEM) with energy dispersive X-ray spectroscopy (EDX), and transmission electron microscopy (TEM). Elemental mappings were performed using a scanning transmission electron microscope (STEM) equipped with a high-angle annular dark-field (HAADF) detector. Samples for TEM analysis was dispersed in ethanol using ultrasonication, and deposited onto a copper grid using a 2.5 mL pipette gun. HR-TEM experiments were conducted using an FEI Titan transmission electron microscope operating at 200 kV. Selected area electron diffraction (SAED) patterns and HRTEM images were acquired using a Gatan Ultra-scan CCD camera and a Gatan K2 direct-detection camera, respectively. ICP measurements were performed using an ICPOES760 instrument (Agilent). Electron spin resonance (ESR) spectra were acquired using a Jeol JES-FA200 spectrometer at

room temperature. UV-vis-NIR spectra were measured using a Thermo Fisher Evolution 201 UV-vis spectrophotometer. Zeta potential was determined using a ZS nanohybrid analyzer (Malvern, England). The concentration of oxygen was detected using a dissolved oxygen instrument (Leici, China). A home-built ^{129}Xe hyperpolarizer was utilized, and all ^{129}Xe NMR/MRI experiments were conducted on a 9.4 T Bruker AV400 wide bore NMR spectrometer (Bruker Biospin, Ettlingen, Germany). Cell apoptosis and necrosis were monitored using a flow cytometer (CytoFLEX, Beckman). Photoacoustic imaging was performed using a MSOT inVision 128 small animal imaging system (MSOT inVision 256-TF, iTheramedical, Germany).

Preparation of PVP-modified Copper sulfide nanoparticles (CuS NPs)

PVP-modified CuS nanoparticles (NPs) were synthesized according to a reported procedure with some modifications.[1] Initially, $CuCl_2 \cdot 2H_2O$ (35 mg) and PVP (200 mg) were dissolved in deionized water (200 mL), followed by sonication until the solution became clear. Subsequently, the mixture was stirred for 30 min at room temperature. Next, Na_2S aqueous solution (800 mL, 60.54 mg mL^{-1}) was added to the mixture, resulting in the solution turning brown. The resulting mixture was stirred for an additional 5 min before being transferred to a polydimethylsiloxane bath at 90°C. After 30 min, the solution turned dark green, indicating the successful synthesis of CuS NPs. The PVP-modified CuS solution was then allowed to cool to room temperature and centrifuged to remove excess free PVP. Finally, the PVP-modified CuS NPs were dispersed in methanol.

Preparation of Cherry-Like CuS in ZIF-8 nanoparticles (CL-CuS-in-ZIF-8 NPs)

To facilitate comparison, the cherry-like CuS in ZIF-8 nanoparticles (designated as CL-in-ZIF-8 NPs) was also synthesized. Initially, $Zn(NO_3)_2 \cdot 6H_2O$ (734.4 mg) was dissolved in methanol (50 mL), followed by the addition of 2-methylimidazole (810.6 mg) in methanol (50 mL) to the pre-prepared CuS NPs methanol solution. Subsequently, the resulting solution was combined with the $Zn(NO_3)_2 \cdot 6H_2O$ methanol solution, stirred until clear, and allowed to stand at room temperature and atmospheric pressure for 24 h. Finally, the residual solvents were

removed under a vacuum at 50°C overnight.

Preparation of Fruitcake-Like CuS embellished ZIF-8 Nanoparticles on ZIF-8 Surface (SL-CuS-on-ZIF-8)

In a typical synthesis of Fruitcake-Like CuS embellished ZIF-8 Nanoparticles on ZIF-8 Surface (designated as SL-CuS-on-ZIF-8), ZIF-8 NPs (50 mg) and CuS NPs (5 mg) were dispersed in 10 mL of deionized water. The solution was stirred overnight, and the liquid was removed using a centrifuge. Subsequently, the obtained products, referred to as SL-CuS-on-ZIF-8 nanoparticles, were dried under vacuum at 50°C overnight.

Preparation of ZIF-8 nanoparticles (ZIF-8 NPs)

ZIF-8 nanoparticles (ZIF-8 NPs) was synthesized following a previously reported procedure with minor adjustments. Typically, $Zn(OAc)_2 \cdot 2H_2O$ (220 mg) and 2-MI (656 mg) were dissolved separately in methanol (50 mL). The 2-MI solution was then added to the $Zn(OAc)_2 \cdot 2H_2O$ methanol solution, and the mixture was stirred for 3 h. Subsequently, the resulting mixture was allowed to stand at room temperature for 24 h. Afterward, the residual solvents were removed using a centrifuge. The obtained products, referred to as ZIF-8 nanoparticles, were then dried under vacuum at 50°C overnight.

Measurement of catalase-like (CAT-like) activity

The catalase (CAT)-like activity of PL-CuS-in-ZIF-8 NPs was evaluated at 25°C by measuring oxygen production with a dissolved oxygen instrument. Specifically, 1 mM H_2O_2 was mixed with NaOAc-HOAc buffer (0.01 M, pH = 7.4), followed by the addition of PL-CuS-in-ZIF-8 NPs (20 mg mL^{-1}). The oxygen concentration was immediately detected, and data were continuously recorded for 10 min. The oxygen production capacity of ZIF-8 NPs (20 mg mL^{-1}) was assessed using similar methods.

Measurement of Peroxidase-like (POD-like) activity

The acetate buffer solution (pH 4.0) containing TMB (2 mM) were mixed with PL-CuS-ZIF-8

(C_{cus} = 80 mg mL^{-1}) plus H_2O_2 (1 mM). The generation of •OH was determined by the absorption increase at 650 nm. The TMB solutions treated with PL-CuS-ZIF-8 or H_2O_2 alone were used as control groups

Measurement of Superoxide Dismutase-like (SOD-like) activity

Methionine (130 mmol L^{-1}) solution, L-methionine (130 mmol L^{-1}) solution, nitroblue tetrazolium (750 mmol L^{-1}) solution, and riboflavin (20 mmol L^{-1}) solution were prepared with PBS (pH = 7.8, 0.05 M). Five finger-shaped glass tubes were employed for the determination, with three serving as measuring tubes and two as control tubes. After mixing, one control tube was kept in darkness, while the other tubes were exposed to a 4000 LUX fluorescent lamp for 15 min. Subsequently, they were immediately transferred to darkness to terminate the reaction. The absorbance values of the remaining tubes were measured at 560 nm, using the non-illuminated tube as a blank reference.

Photothermal effect of PL-CuS-in-ZIF-8 NPs

To investigate the photothermal effect of PL-CuS-in-ZIF-8 aqueous solution, experiments were conducted to vary the sample concentration, adjust the laser power, and assess photostability. Initially, the sample concentration was altered, and the sample was exposed to an 808 nm NIR laser (2 W cm^{-2}) for 5 min. Subsequently, the laser power was adjusted to maintain the sample concentration at 1 mg mL^{-1}, with a laser power range of 0 to 2 W cm^{-2} for 5 min. Finally, the sample underwent irradiation with an 808 nm laser (1 mg mL^{-1}) at a power of 2 W cm^{-2} for 5 min, followed by a 15-min pause, and repeated for 5 cycles to evaluate the photostability of the sample. Temperature changes in the solution were continuously monitored throughout the experiment using an IR thermal imaging system (Wuhan Hot Sight Technology Co., Ltd.) and recorded every 30 seconds. Then, the photothermal conversion efficiencies (h) were analyzed using the following equation:

$$\eta = \frac{hs(T_{max} - T_{surr}) - Q_{dis}}{I(1 - 10^{-A_\lambda})}$$

T_{max} is the equilibrium temperature of the sample solution, and T_{sur} corresponds to the

environmental temperature of the experiment. Q_{dis} corresponds to the heat loss resulting from the absolotion of light by the container, according to $Q_{dis}= I(5.4x10^{-4})$. I represents the power density (2 W cm^{-2}) of the 808 nm laser, and the absorbance of the sample solution at 808 nm was recorded as A_l. The value of *hs* can be calculated by the next formula:

$$hs = \frac{mC_{water}}{\tau_s}$$

Here, m represents the mass of the sample solution and C_{water} corresponds to the heat capacity of water (4.2 $Jg^{-1}K^{-1}$). τ_s is the time constant of the system. The value of *hs* can be calculated by the next formula:

$$t = -\tau_s \ln\theta = -\tau_s \ln\left(\frac{T - T_{surr}}{T_{max} - T_{surr}}\right)$$

T is the temperature of natural cooling to room temperature.

Photoacoustic Performance of PL-CuS-in-ZIF-8 NPs

To assess the photoacoustic performance of the nanoparticles, solutions of PL-CuS-in-ZIF-8 NPs with concentrations ranging from 10 to 150 mg mL^{-1} were prepared. These solutions were then analyzed using an MSOT inVision 256-TF small animal imaging system (iThera Medical GmbH, Munich, Germany) for photoacoustic imaging.

Cell Culture

Cell experiments were conducted on A549 cells (a human non-small cell lung cancer cell line). A549 cells were obtained from the Cell Bank of the Chinese Academy of Sciences (Shanghai, China). The cells were cultured in F12K medium containing 10% FBS and 1% penicillin-streptomycin under incubation conditions of 37°C and 5.0% CO_2.

In Vitro Cytotoxicity Studies

The A549 and BEAS-2B cells were seeded into 96-well plates at a density of 10^4 cells per well in the F12K for 24 h to allow for cell attachment. The culture medium was then replaced with fresh medium containing serial dilutions of varying concentrations of PL-CuS-in-ZIF-8 NPs. After an additional 4 h incubation, CCK-8 was added to the medium, and cells were

incubated at 37°C for 30 min. The absorbance at 450 nm was measured using a microplatereader (SpectraMax 190, Molecular Devices). Herein, all data were conducted through six independent parallel experiments The cell inhibition rate was calculated using the following equation:

$$Cell\ inhibition\ rate\ (\%) = \frac{A_{sample} - A_{blank}}{A_{positive} - A_{blank}} \times 100$$

where $A_{positive}$, A_{blank}, and A_{sample} represent the absorbance of the positive control group (pure culture media), blank control group (culture medium without cells or drugs), and sample group, respectively.

In Vitro Cellular Uptake Assay

The cellular uptake ability of PL-CuS-in-ZIF-8 NPs in vitro was observed using a fluorescence inverted microscope (A1R/A1, Nikon, Japan). Indocyanine green (ICG) was utilized as a fluorescent probe to label the nanoparticles for detection. PL-CuS-in-ZIF-8@ICG was prepared by dispersing 1 mg ICG and 50 mg PL-CuS-in-ZIF-8 NPs in deionized water and stirring in the dark for 5 h. The resulting solution was then collected to obtain the product. Similarly, PL-CuS-in-ZIF-8@Rhodamine B was prepared.

A549 cells were seeded in 6-well plates at a density of 1 × 10^5 cells/well and cultured overnight. The medium was then replaced with 2 mL of fresh cell medium containing 50 mg mL^{-1} PL-CuS-in-ZIF-8@ICG. After 4 h of incubation, the medium was removed, and 200 mL of DAPI staining solution was added to each well and incubated for 2 min before removal. The cells were washed three times with PBS. In vitro cell uptake experiments were conducted for PL-CuS-in-ZIF-8@Rhodamine B following the same method as for PL-CuS-in-ZIF-8@ICG. Cells were incubated with appropriate concentrations of phalloidin-FITC, DAPI, and PL-CuS-in-ZIF-8@Rhodamine B, stained and washed sequentially, and the cellular uptake behavior was observed under a fluorescence inverted microscope and photographed.

In Vitro Cellular Live and Death

Briefly, A549 cells (1 × 10^5) were seeded into 6-well plates and incubated with serum-free

medium containing either PL-CuS-in-ZIF-8 (100 mg mL^{-1}) or PBS (pH 7.4, 10 mM) for 4 h. After washing the cells three times with PBS, they were either exposed to 808 nm laser irradiation (1 W cm^{-2}) for 5 min or left untreated. Subsequently, the cells were stained with Calcein AM/PI to identify living cells (green) and dead cells (red), and imaged using a confocal laser scanning fluorescence microscope (A1R/A1, Nikon, Japan).

Lysosomal Membrane Permeabilization

A549 cells were seeded in confocal dishes and incubated for 24 h. Following this incubation period, the cells were treated for an additional 24 h with PL-CuS-in-ZIF-8 (100 mg mL^{-1}) and ZIF-8 (100 mg mL^{-1}). Subsequently, the cells were stained with acridine orange (AO) at a concentration of 5 mM for 30 min and imaged using confocal laser scanning microscopy (CLSM). The excitation wavelength was set at 488 nm, and emissions were captured at 488 nm for the green channel and 561 nm for the red channel.

The Evaluation of Intracellular Pyruvate, a-Ketoglutaric Acid and Succinic Acid

A549 cells were treated with PBS and PL-CuS-in-ZIF-8 (100 mg mL^{-1} in MEM) for 2 h. Subsequently, the intracellular levels of pyruvate, a-ketoglutaric acid, and succinic acid were measured using appropriate assay kits, following the manufacturer's instructions.

Intracellular Zn^{2+} ions detection

Intracellular Zn^{2+} ions detection was examined by a Zn^{2+} ions probe [N-(6-Methoxy-8-quinolyl)-p-toluenesulfonamide] (TSQ, MedChemExpress). A549 cells were seeded into 6-well plates at the density of 1×10^5 cells per well (1 mL of F12K) and then incubated with Control, PL-CuS-in-ZIF-8 NPs (50 μg mL^{-1}), for 0, 1 h, 2 h, and 4 h, respectively. Then 1 μL of TSQ DMSO solution (0.1 M) was added and then the 6-well plate was incubated for 30 min at 37 ℃. Next, the culture media were replaced and washed by fresh PBS and then observed under inverted fluorescence microscope (Nikon).

Detection of Intracellular Protein Expression

A549 cells were seeded into 6-well plates for 24 h. Subsequently, cells were treated with PL-CuS-in-ZIF-8, PL-CuS-in-ZIF-8 + Laser at specified concentrations for 2 h. Following treatment, cells were washed thrice with cold PBS and lysed with ice-cold lysis buffer for western blot (Pinuofei, China). Protein concentration was determined using the bicinchoninic acid (BCA) method. After boiling in loading buffer (Pinuofei, China), aliquots of each protein sample were separated by SDS-PAGE using precast Bis-Tris 8-20% gels in MOPS Running Buffer (Pinuofei, China). Separated proteins were transferred onto polyvinylidene fluoride (PVDF) membranes. The membranes were then blocked with 5% BSA in Tris Buffered Saline Tween (TBST) for 1 h at room temperature and subsequently immunoblotted with primary antibodies, including DLAT (1:2000, Proteintech), or Actin (1:2000, abclonal), at 4°C overnight. The following day, membranes were washed five times with TBST. Protein bands were visualized using an Enhanced Chemiluminescence (ECL) Substrate Kit (Guangdong Yuehua Medical Instrument Factory Co., Ltd).

Histologic Evaluation and Immunofluorescence

Organ samples were fixed in 4% paraformaldehyde and subjected to H&E, TUNEL, Ki67, FDX1, DLAT, and ROS staining. H&E staining assessed organ damage, TUNEL and Ki67 evaluated tumor proliferation, FDX1 and DLAT assessed copper death processes, while ROS staining observed the chemodynamic therapy (CDT) process (Wuhan Pinuofei Biological Technology Company). Cells were treated with 10% horse serum and 0.3% Triton X-100 in PBS (A110694-0500; Synon Biotechnology, Shanghai, China) for 1 h, followed by staining with rabbit anti-FDX1 and rabbit anti-DLAT (abclonal, China) overnight. Finally, samples were treated with secondary antibodies and DAPI. Slides were mounted with anti-fluorescence mounting medium (Dako, S3023), and images were captured with a fluorescence microscope.

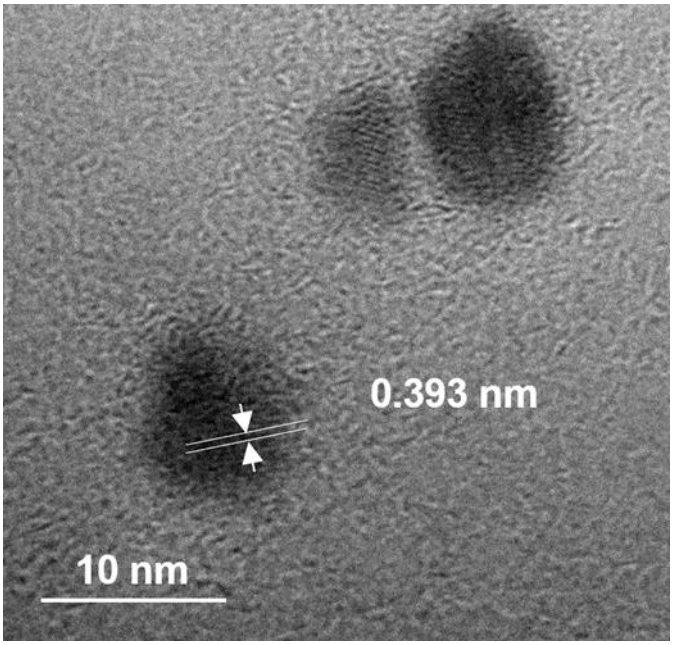

Figure S1. TEM image of the CuS NPs.

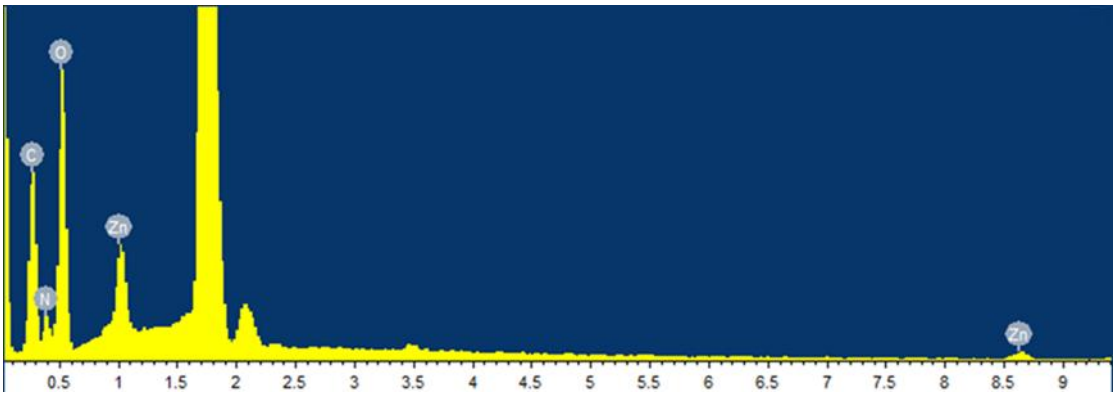

Figure S2. Energy Dispersive X-ray Spectroscopy (EDS) analysis of PL-CuS-in-ZIF-8 from SEM.

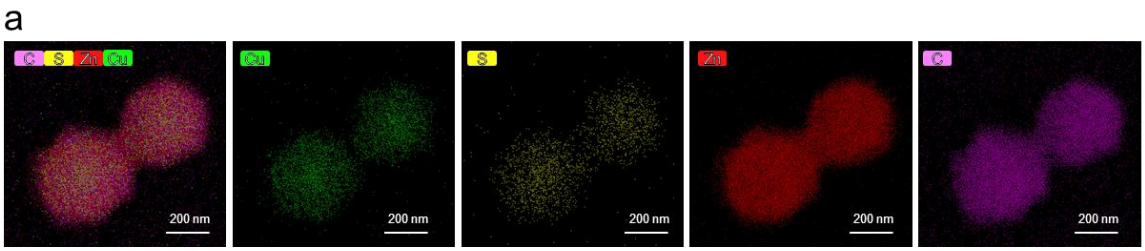

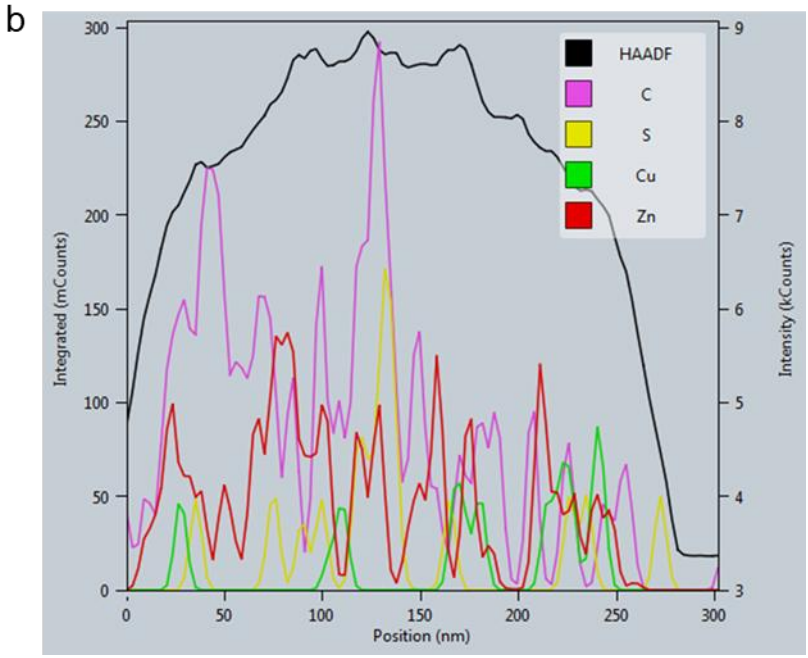

Figure S3. High-resolution electron microscopy imaging and elemental mapping analysis of PL-CuS-in-ZIF-8. a) mapping, b) line scan.

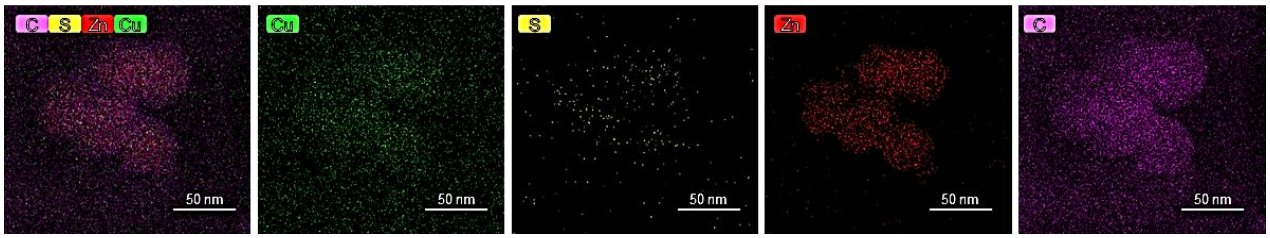

Figure S4. High-resolution electron microscopy imaging and elemental mapping analysis of CL-CuS-in-ZIF-8.

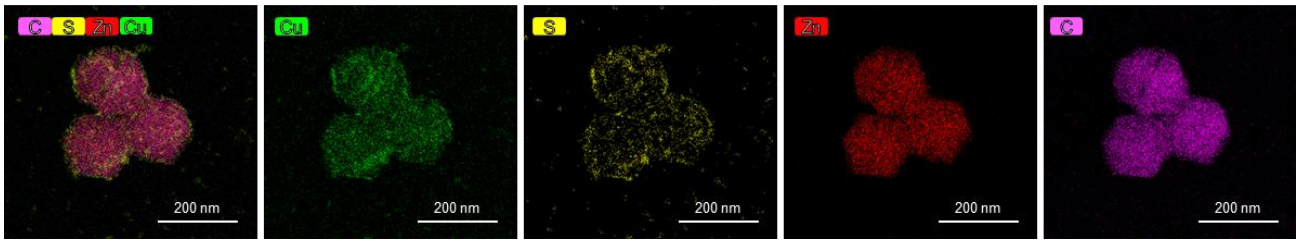

Figure S5. High-resolution electron microscopy imaging and elemental mapping analysis of SL-CuS-on-ZIF-8.

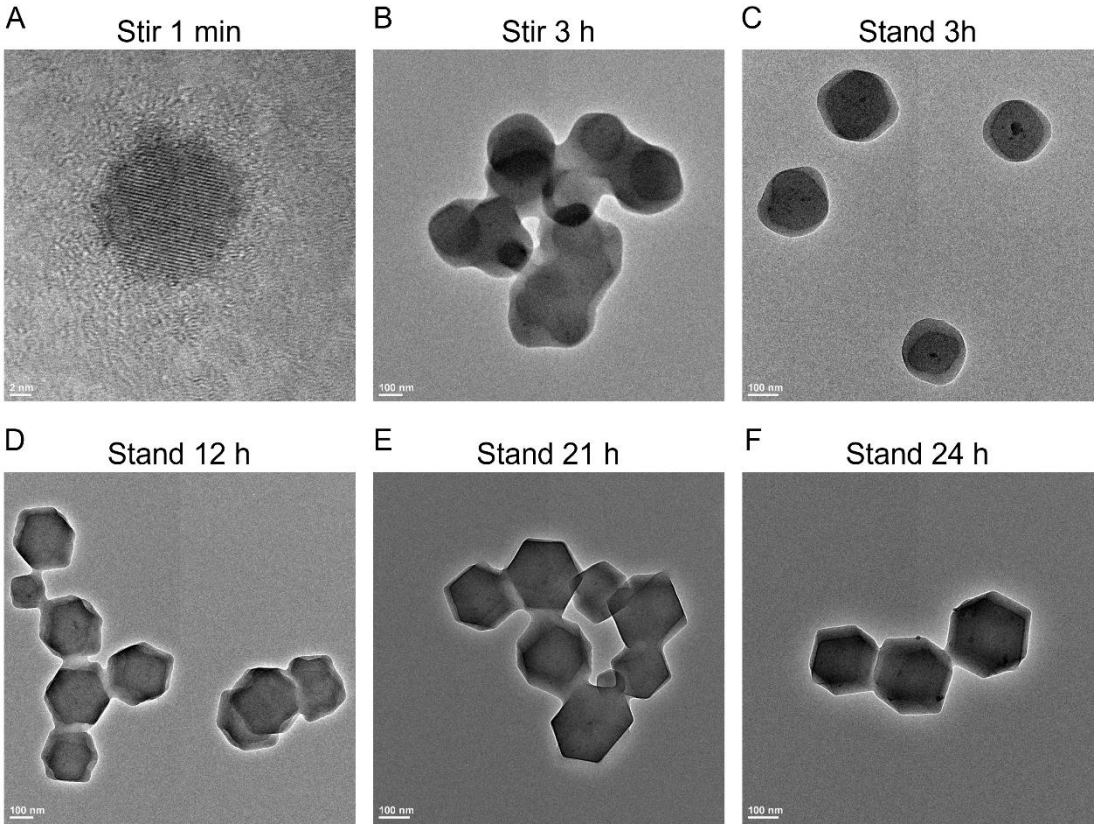

Figure S6. TEM analysis of CuS NPs encapsulation within ZIF-8 crystals.

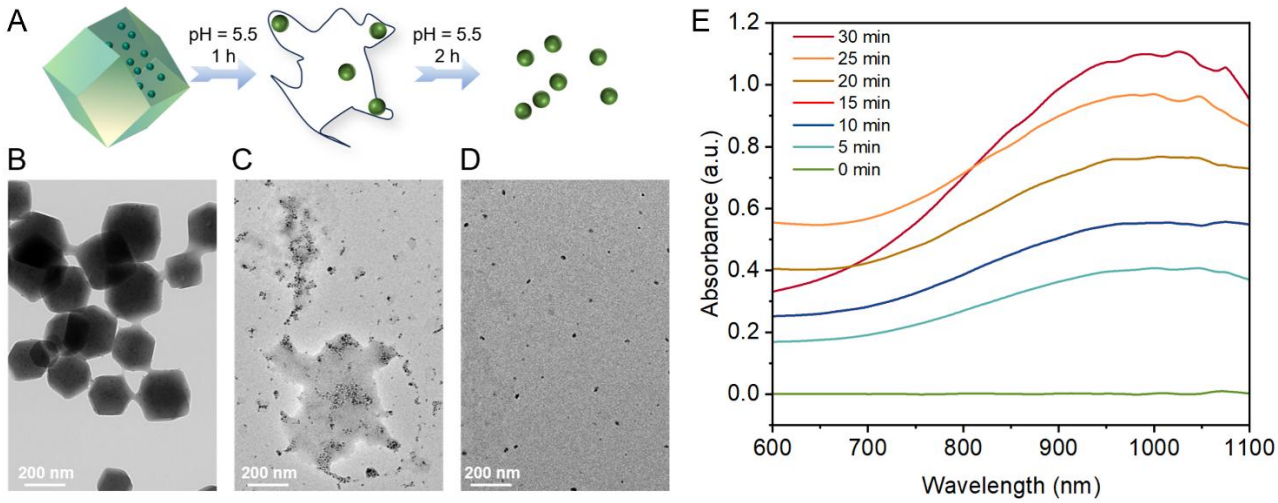

Figure S7. TEM analysis and UV-vis absorption spectroscopy of PL-CuS-in-ZIF-8 NPs under weakly acidic conditions. (A) schematic diagram of the release process. (B) pristine PL-CuS-

in-ZIF-8 NPs. (C) after 1 h incubation in pH 5.5 buffer. (D) after 2 h incubation in pH 5.5 buffer. (E) UV-vis absorption spectra of the CuS NPs in the liquid supernatant at different time points.

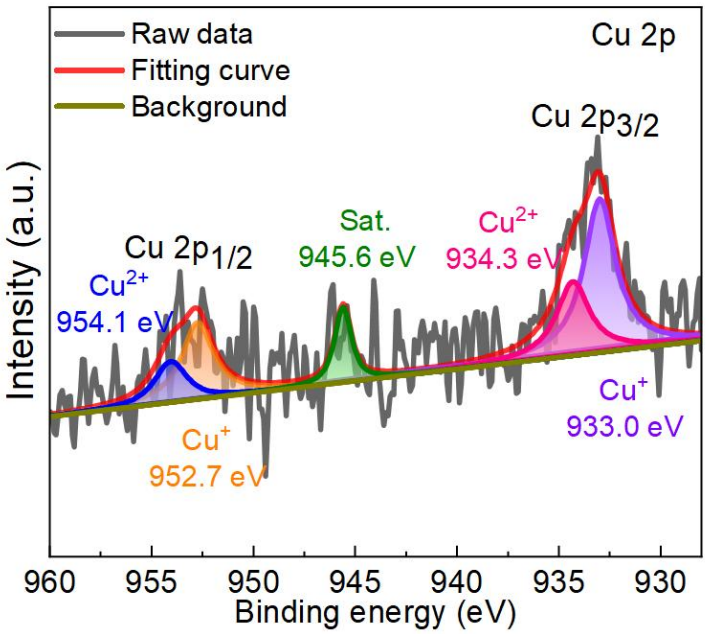

Figure S8. XPS analysis of the oxidation state of Cu in PL-CuS-in-ZIF-8.

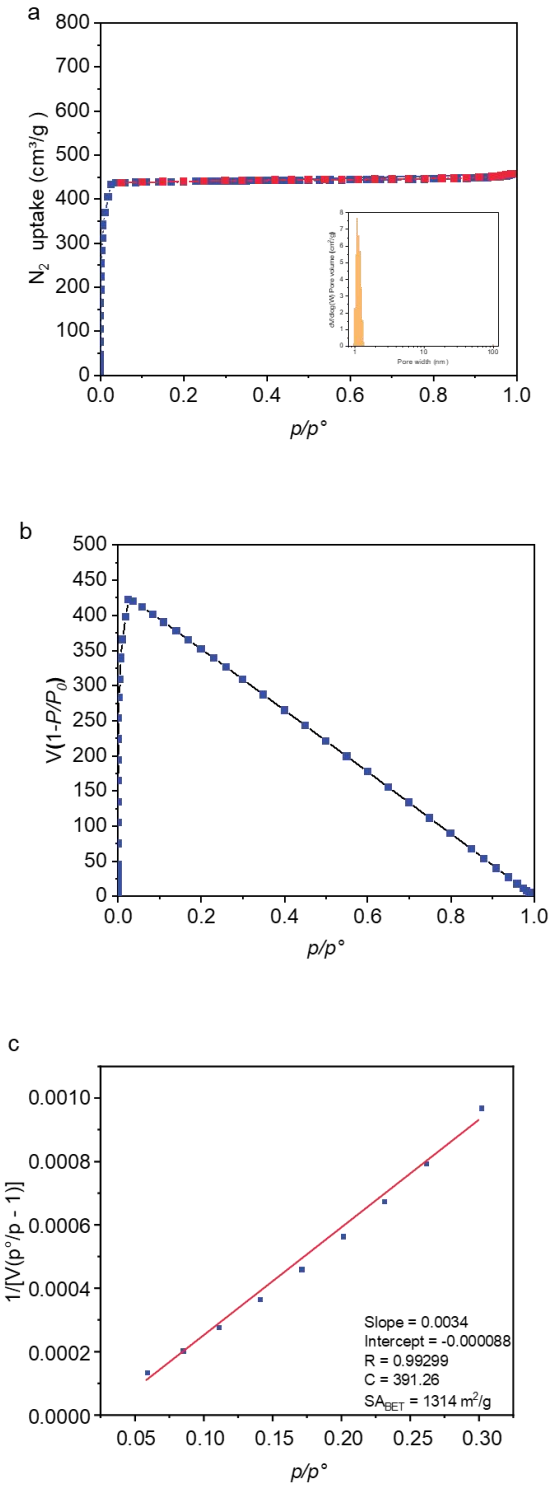

Figure S9. a) adsorption Isotherm of ZIF-8 nanoparticles at 77 K (the internal figure depicts the pore size distribution). b) fitting of the nitrogen adsorption curve for ZIF-8 particle size. c) selection of points for BET specific surface area calculation.

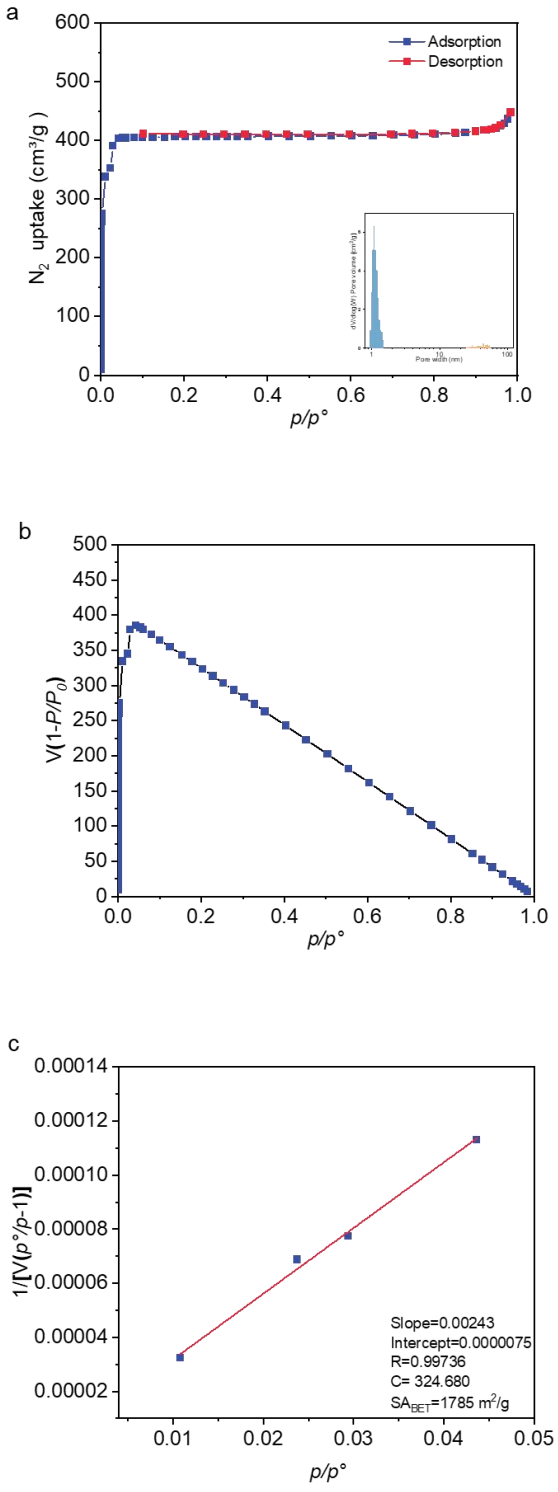

Figure S10. a) adsorption Isotherm of PL-CuS-in-ZIF-8 nanoparticles at 77 K (the internal figure depicts the pore size distribution). b) fitting of the nitrogen adsorption curve for PL-CuS-in-ZIF-8 particle size. c) selection of points for BET specific surface area calculation.

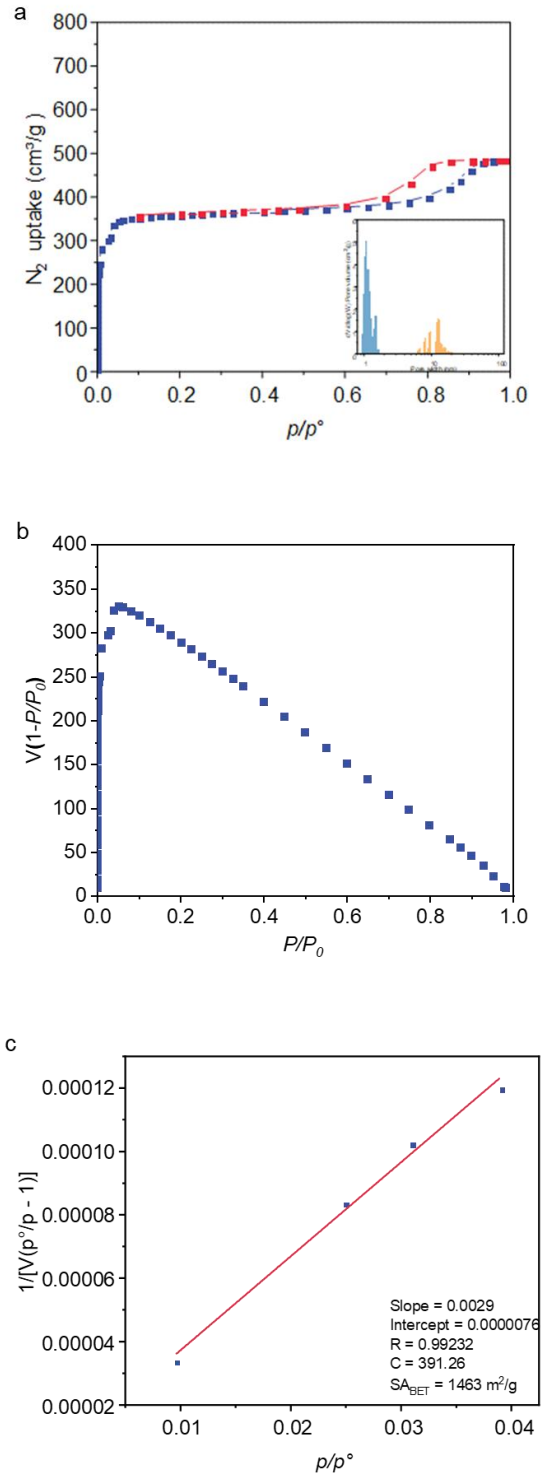

Figure S11. a) adsorption Isotherm of CL-CuS-in-ZIF-8 nanoparticles at 77 K (the internal figure depicts the pore size distribution). b) fitting of the nitrogen adsorption curve for CL-CuS-in-ZIF-8 particle size. c) selection of points for BET specific surface area calculation.

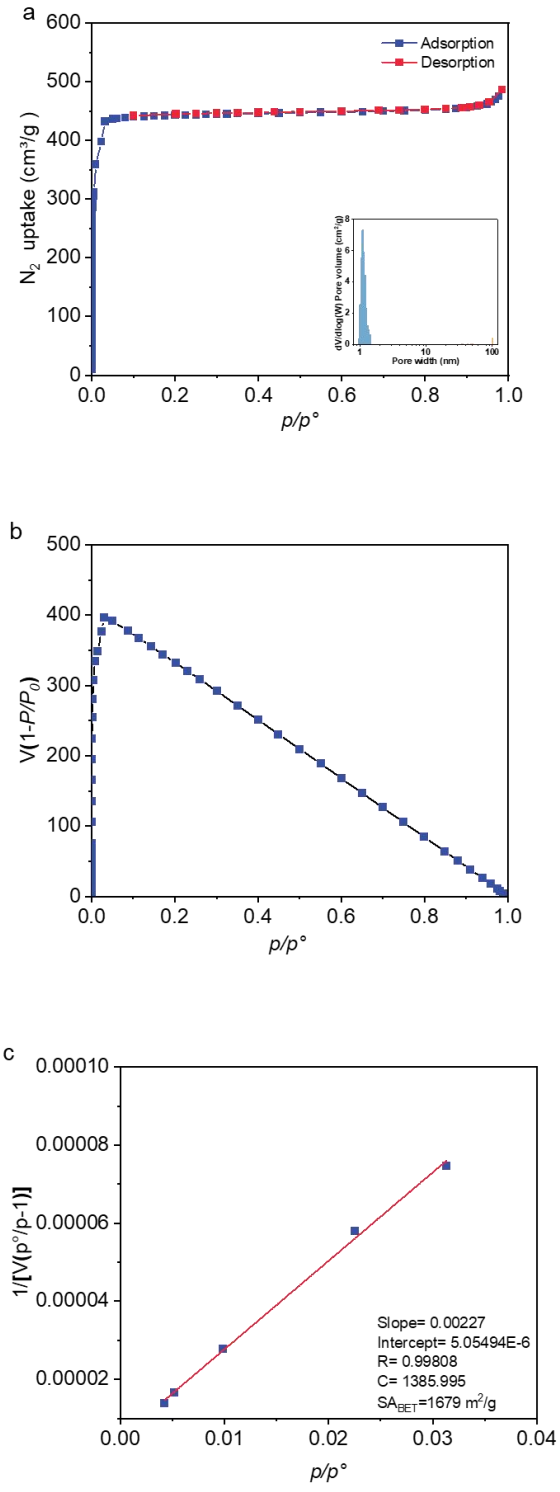

Figure S12. a) adsorption Isotherm of SL-CuS-on-ZIF-8 nanoparticles at 77 K (the internal figure depicts the pore size distribution). b) fitting of the nitrogen adsorption curve for SL-CuS-on-ZIF-8 particle size. c) selection of points for BET specific surface area calculation.

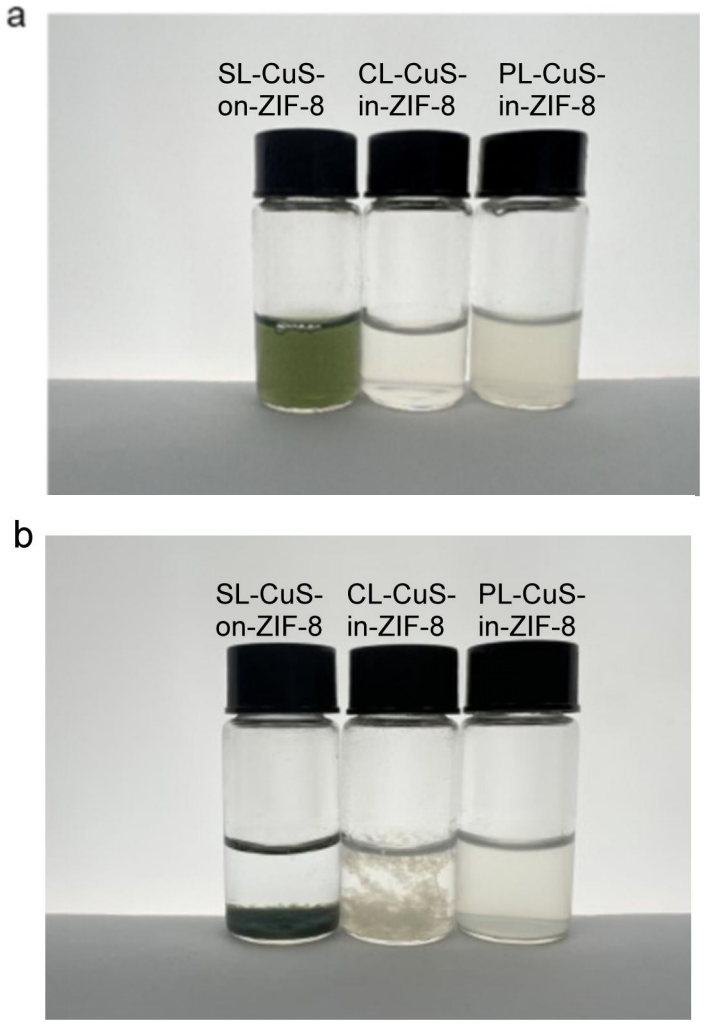

Figure S13. Various nanoparticle types were suspended in water and left undisturbed for a period. From left to right, the nanoparticles are designated as SL-CuS-on-ZIF-8, CL-CuS-in-ZIF-8, and PL-CuS-in-ZIF-8, respectively. (a) represents the initial state (b) depicts the state after two days of standing.

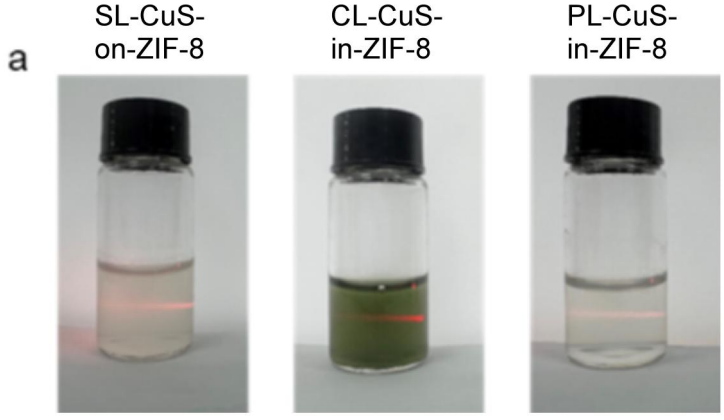

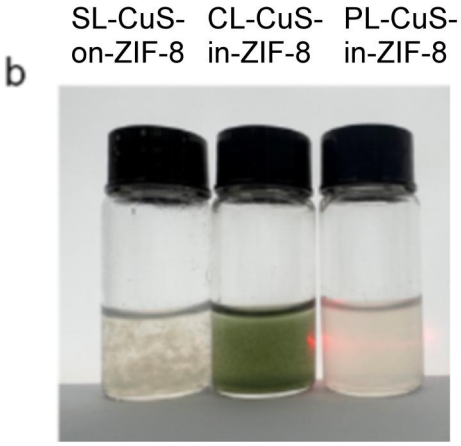

Figure S14. Tyndall effect exhibited by different types of nanoparticles dispersed in water. (a) represents the initial state (b) depicts the state after two days of standing.

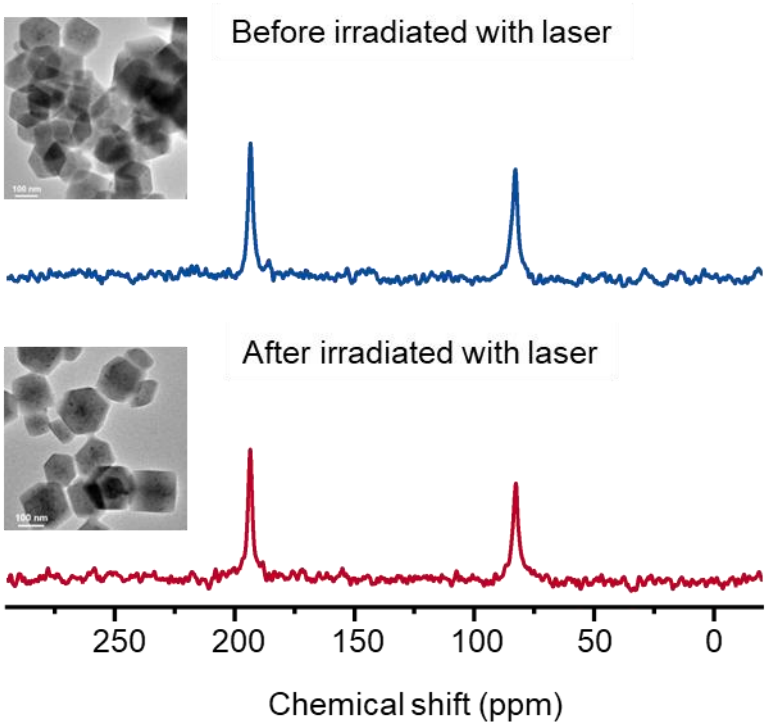

Figure S15. The ^{129}Xe NMR spectrum of PL-CuS-in-ZIF-8 before laser irradiation (blue) and after laser irradiation (red), along with the corresponding TEM image in the small panel on the left.

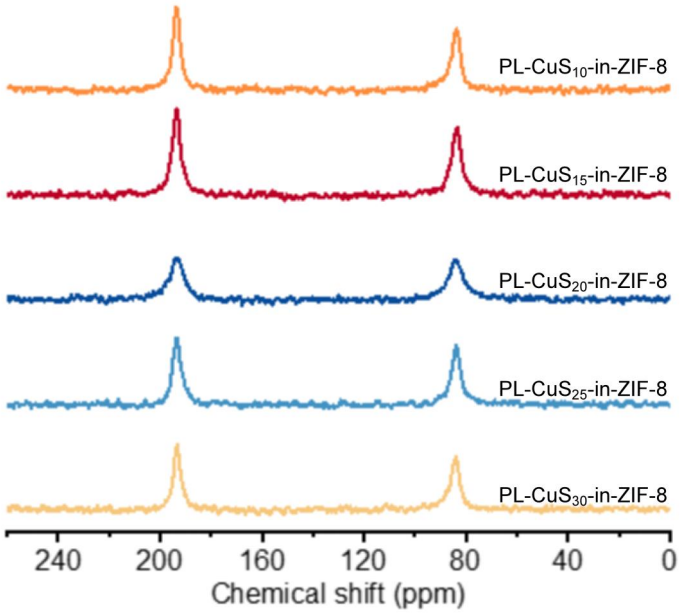

Figure S16. The ^{129}Xe NMR spectrum of different PL-CuS-in-ZIF-8.

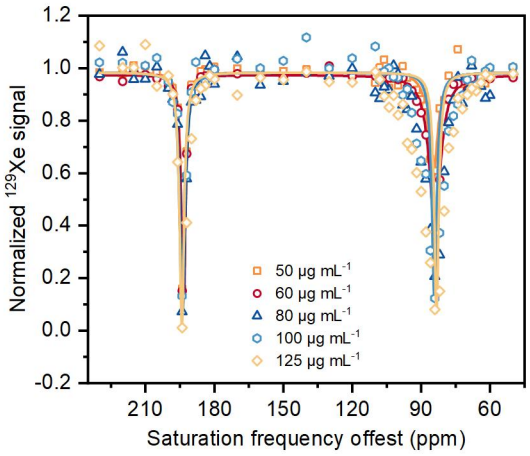

Figure S17. Hyper-CEST of PL-CuS-in-ZIF-8 at low concentration.

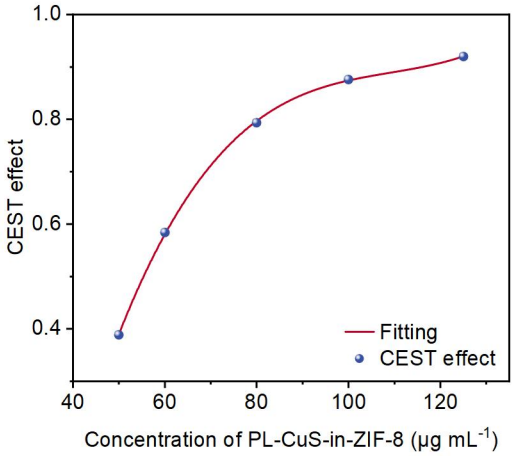

Figure S18. Relationship between Hyper-CEST effect and concentration of PL-CuS-in-ZIF-8.

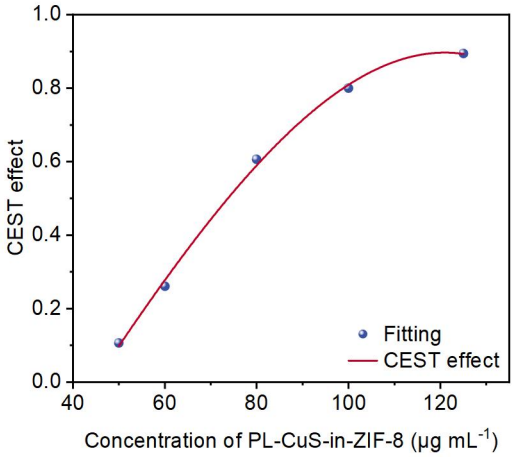

Figure S19. Relationship between MRI signal intensity effect and concentration of PL-CuS-in-ZIF-8.

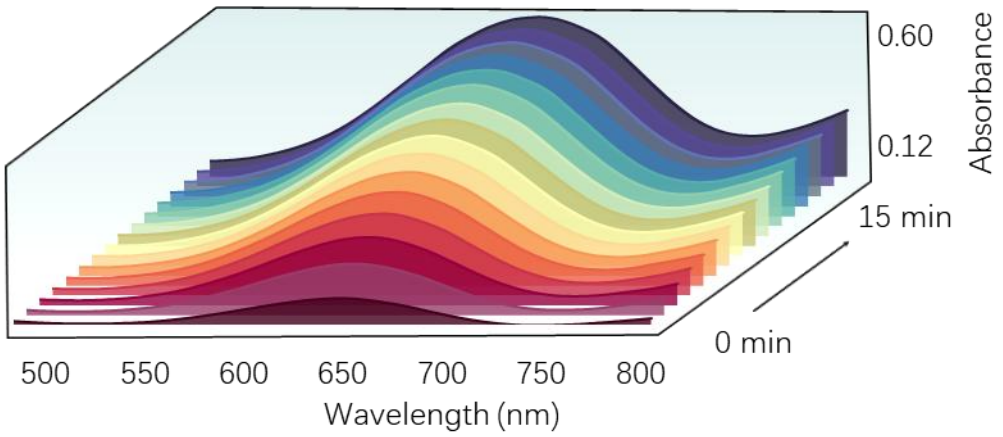

Figure S20. UV-vis spectra of PL-CuS-in-ZIF-8 conjugated with 3,3',5,5'-Tetramethylbenzidine (TMB) in the presence of H_2O_2 at pH 4.0 were recorded within 15 min.

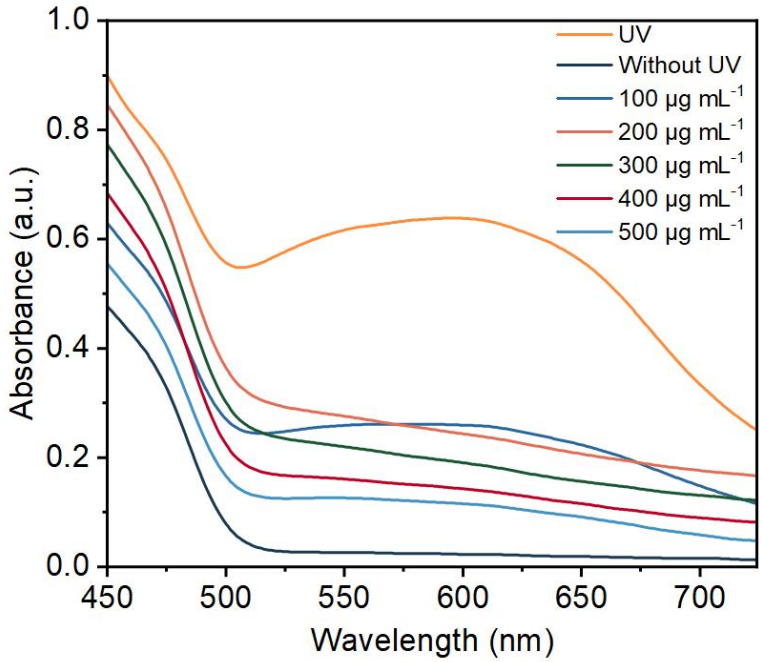

Figure S21. The UV-vis spectra of PL-CuS-in-ZIF-8 conjugated with Nitroblue tetrazolium chloride (NBT) show the formation of a blue methylhydrazine upon irradiation, with maximal absorption observed at 560 nm.

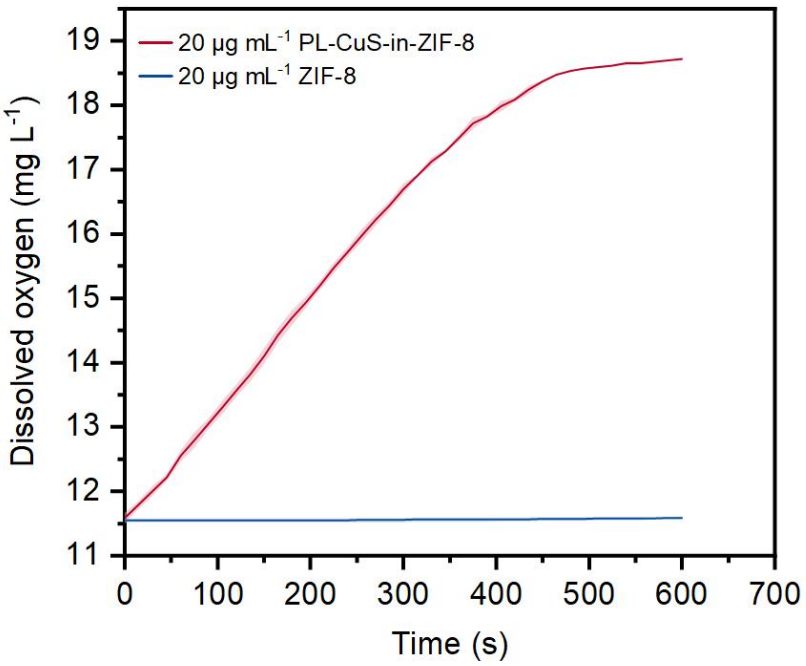

Figure S22. The oxygen content of PL-CuS-in-ZIF-8 in the presence of H_2O_2.

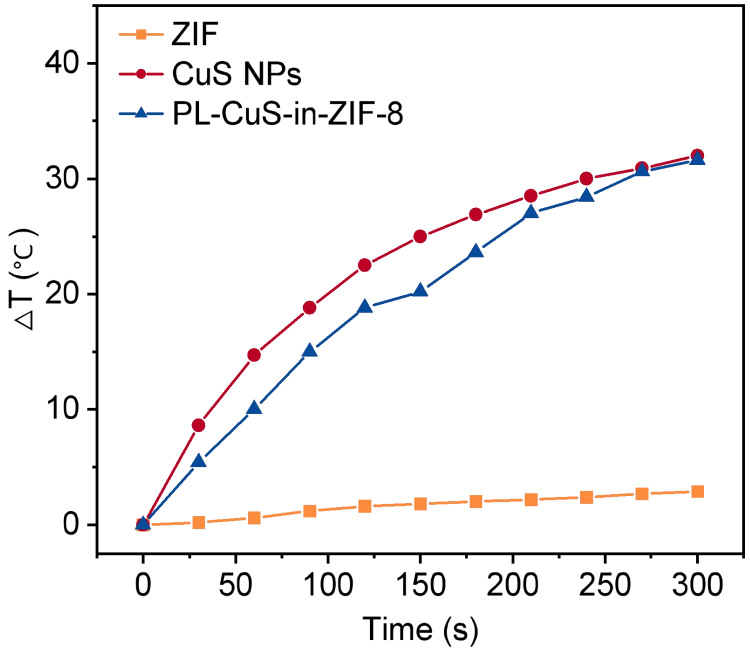

Figure S23. ZIF-8, CuS NPs and PL-CuS-in-ZIF-8 (C_{CuS} = 40 mg mL^{-1}) were irradiated by 2 W cm^{-2} laser.

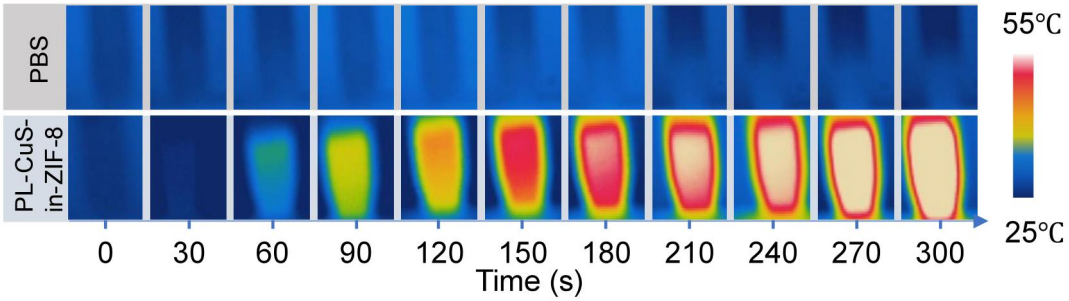

Figure S24. ZIF-8 and PL-CuS-in-ZIF-8 (C_{CuS} = 40 mg mL^{-1}) were irradiated by a 2 W cm^{-2} laser.

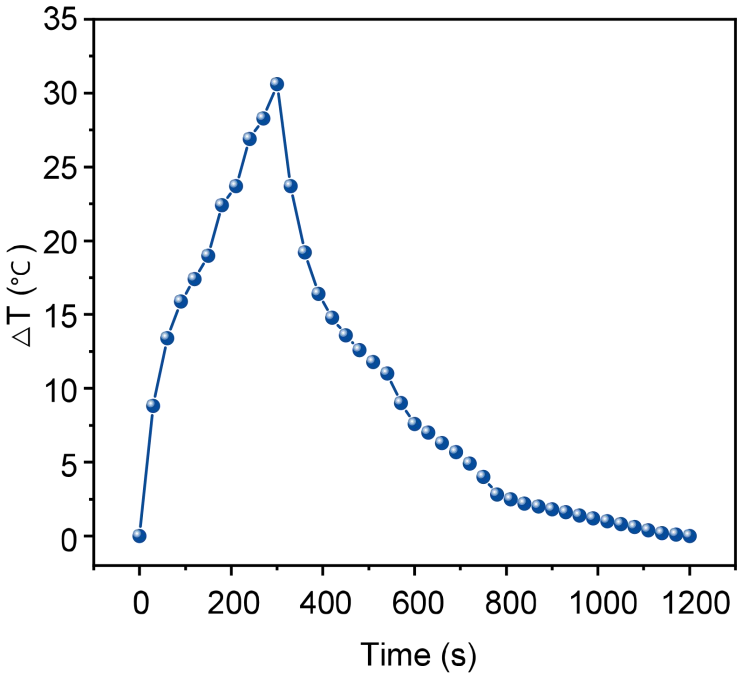

Figure S25. Photothermal heating curve to calculate the photothermal conversion efficiency. PL-CuS-in-ZIF-8 were irradiated by 808 nm laser with a power density of 2 W cm^{-2} to reach a temperature plateau; then, the laser was shut off and the temperature was allowed to cool to room temperature naturally.

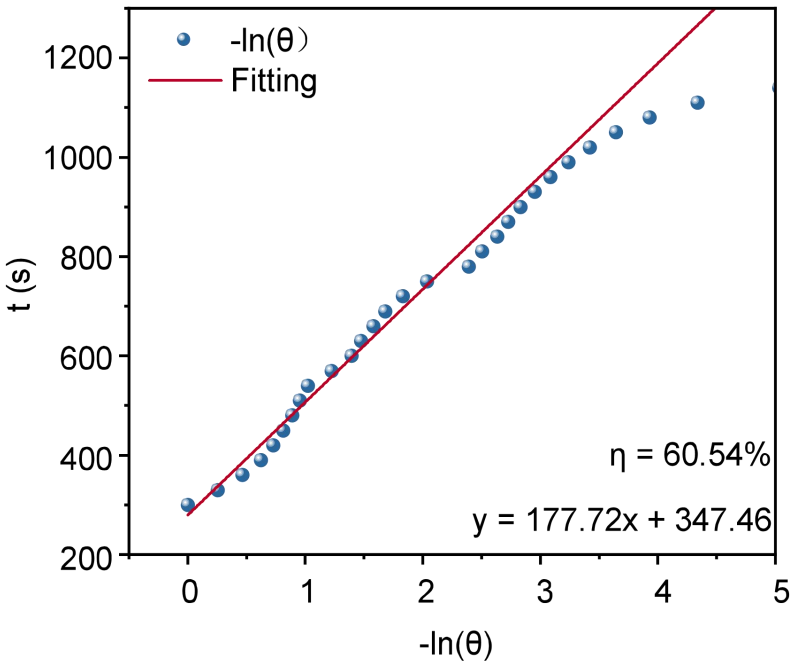

Figure S26. The plot of linear time data from the cooling period of PL-CuS-in-ZIF-8 NPs versus negative natural logarithm of the driving force temperature (q).

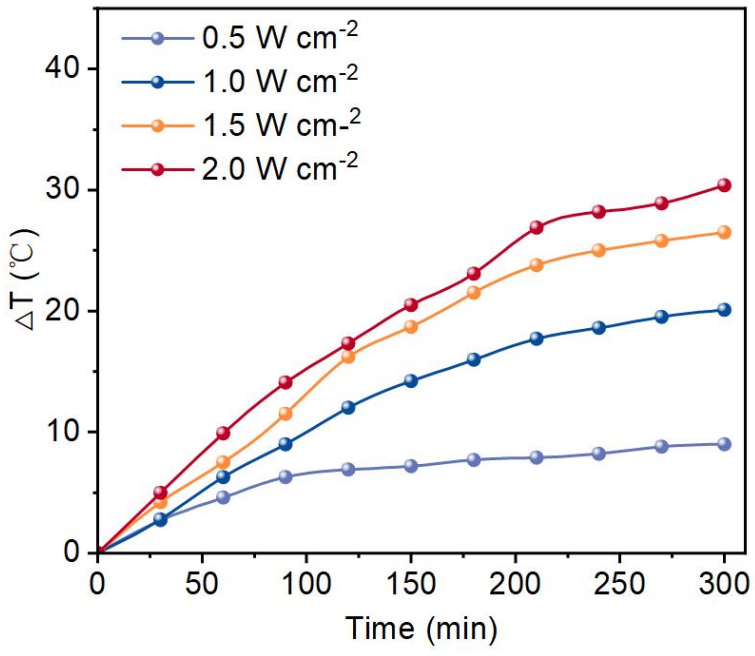

Figure S27. Laser irradiation with different power was performed in C_{CuS} = 40 mg mL^{-1} aqueous solution of PL-CuS-in-ZIF-8.

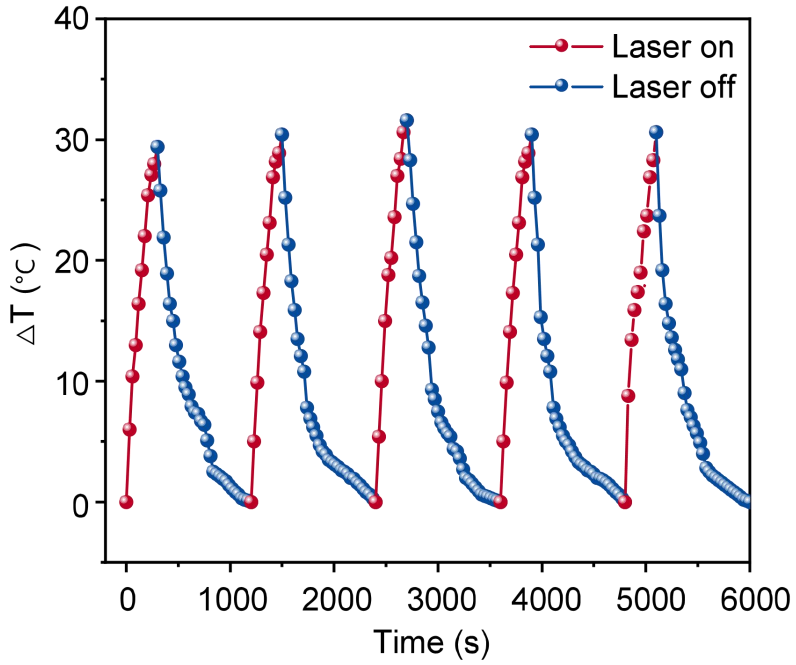

Figure S28. PL-CuS-in-ZIF-8 shows excellent photostability upon 808 nm laser irradiation at the power density of 2 W cm^{-2} for 5 min after five heat−cool cycles.

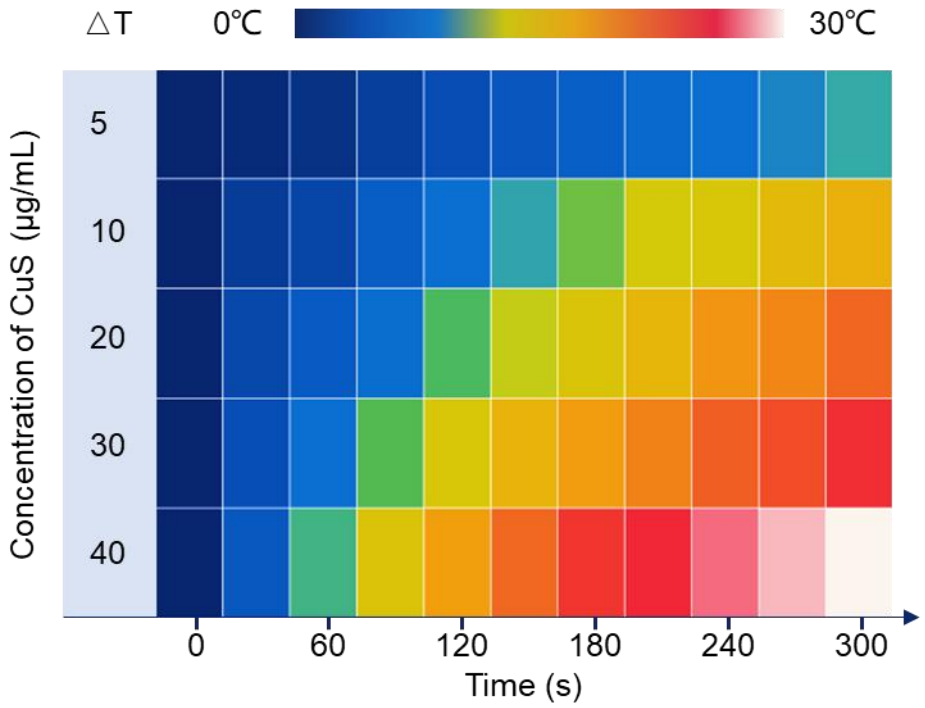

Figure S29. Different concentrations of solution PL-CuS-in-ZIF-8 were irradiated with 2 W cm^{-2} laser for 5 min.

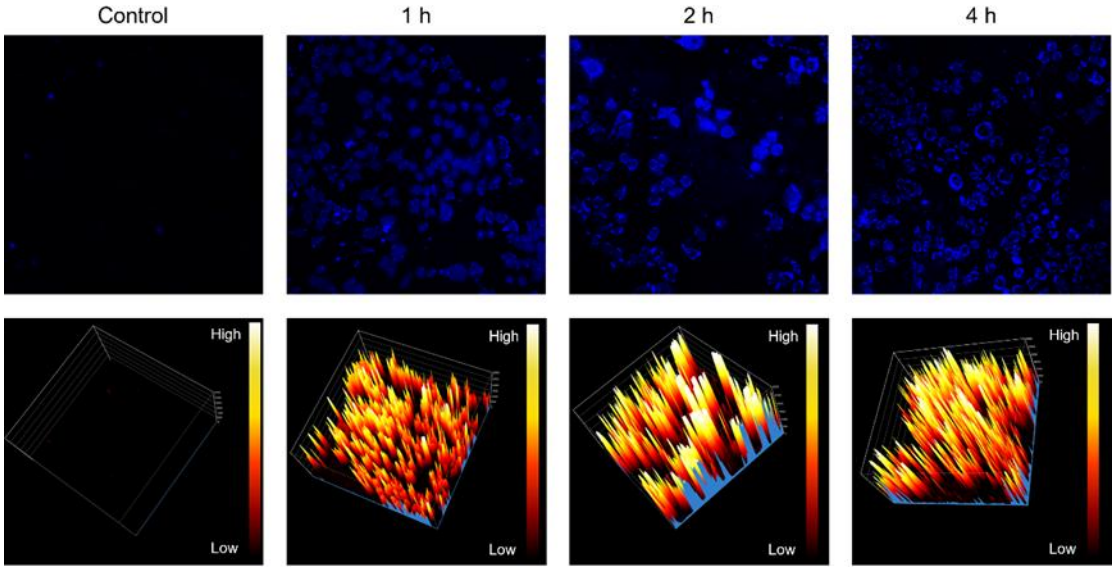

Figure S30. Intracellular Zn^{2+} detections with different time points.

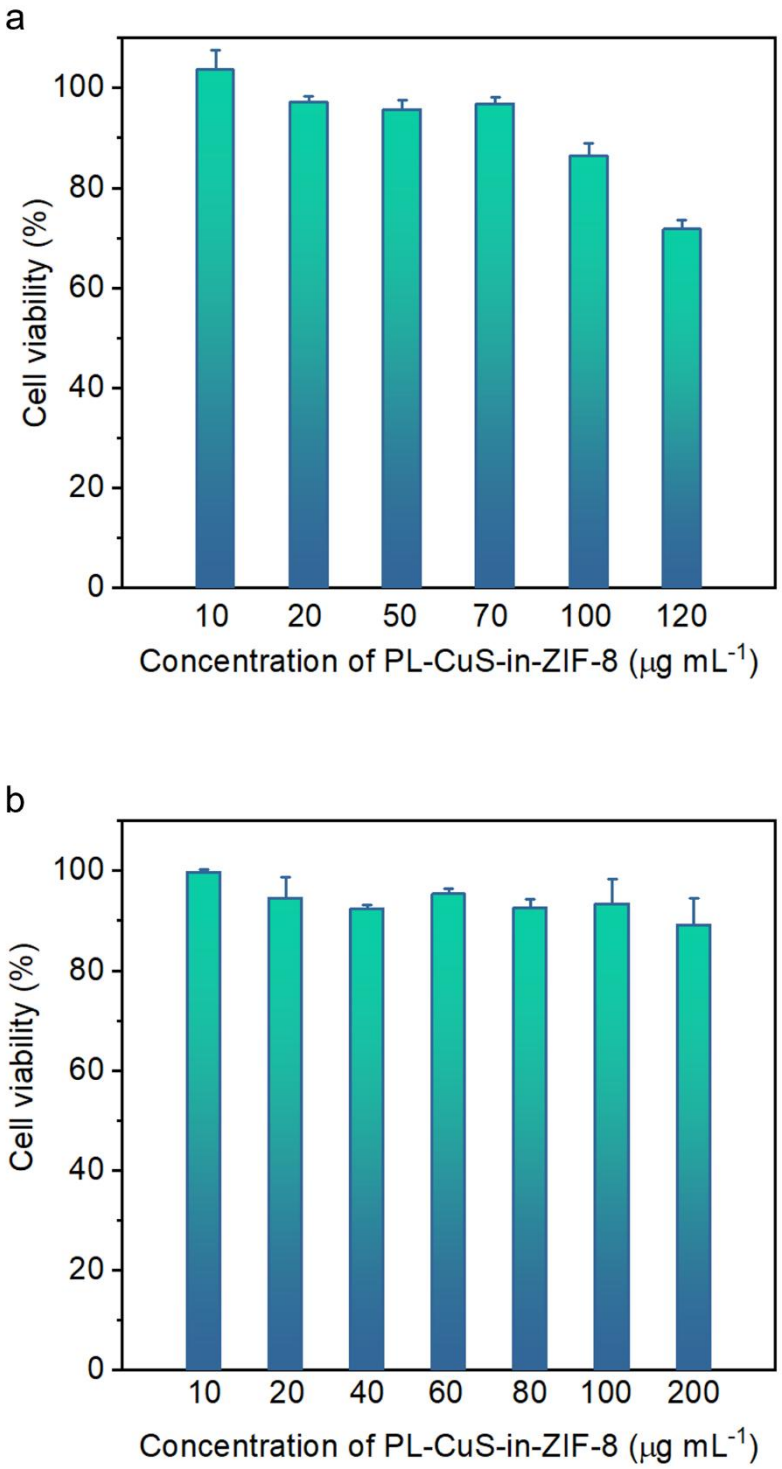

Figure S31. CCK-8 assay demonstrating cell viability, a) A549 cells, b) BEAS-2B cells. Data are shown as mean ± SD, n=3.

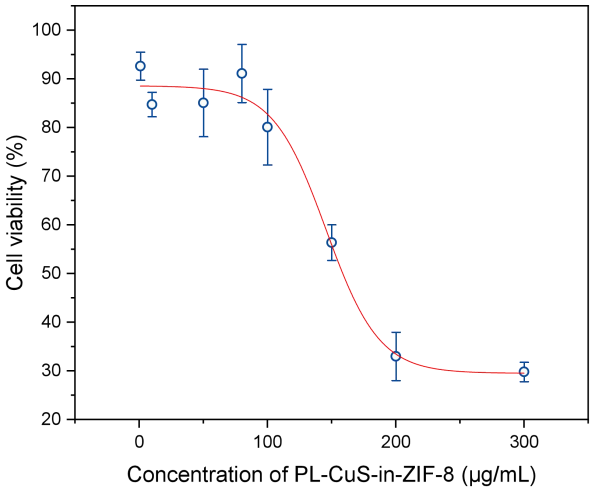

Figure S32. CCK-8 assay for PL-CuS-in-ZIF-8-treated tumor cells for 24 h. Data are shown as mean ± SD, n=3.

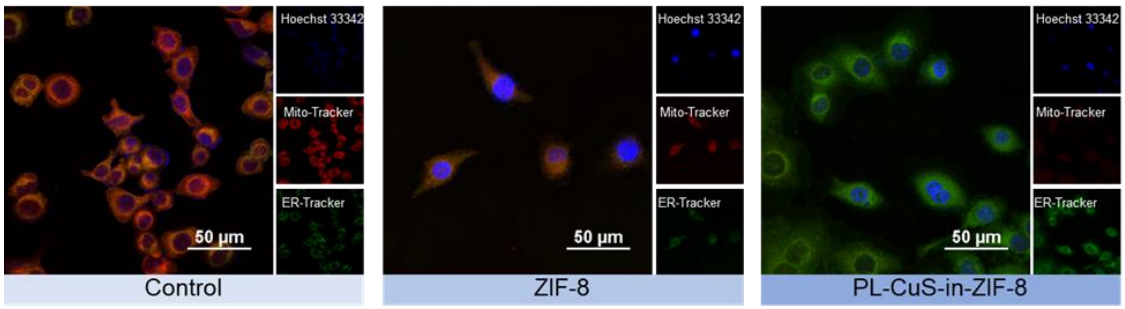

Figure S33. CLSM images analyzed mitochondria and endoplasmic reticulum of A549 cells.

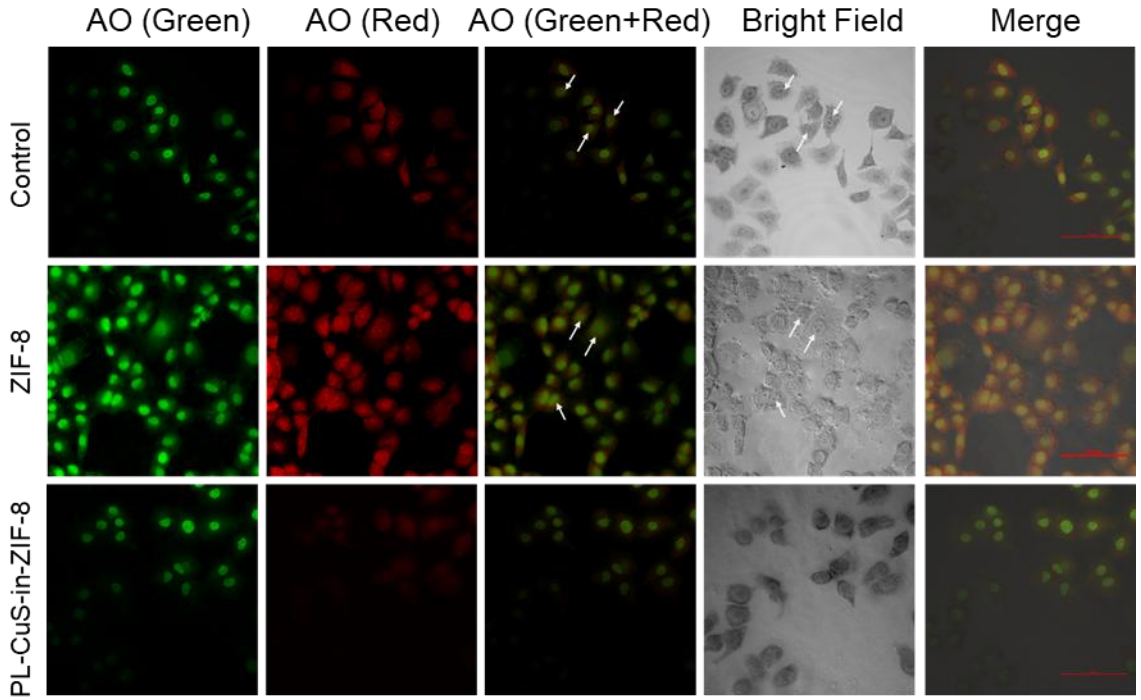

Figure S34. Confocal laser scanning microscopy (CLSM) images depict acridine orange (AO)-stained A549 cells after 2 h of incubation with or without PL-CuS-in-ZIF-8 and ZIF-8. The scale bar corresponds to 100 mm, and white arrows highlight AO accumulation in intact lysosomes (scar bar = 100 mm).

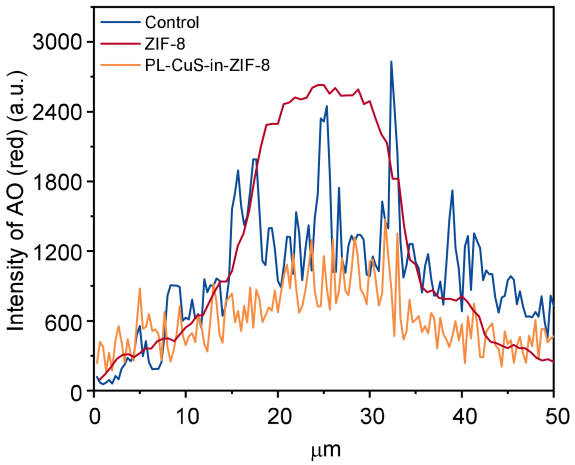

Figure S35. Intensity of AO (red).

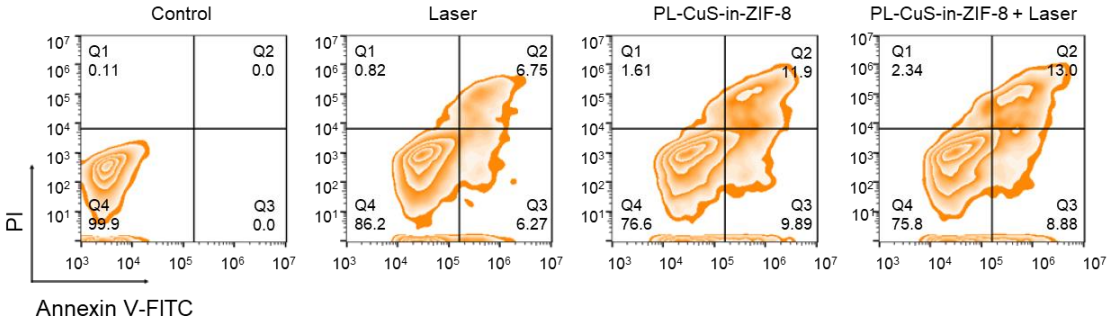

Figure S36. Flow cytometry was conducted using Annexin V-FITC and PI.

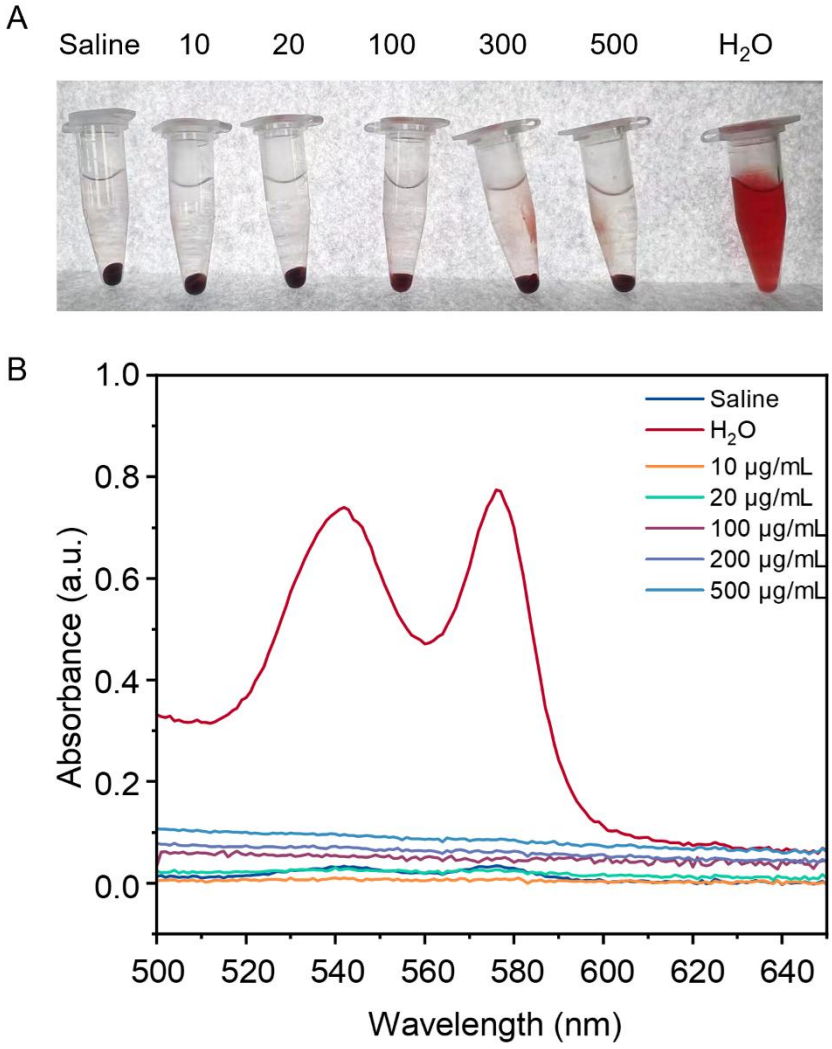

Figure S37. Hemolysis assay. (A) Images of blood samples after various treatments. (B) Absorbance of the supernatant following different treatments.

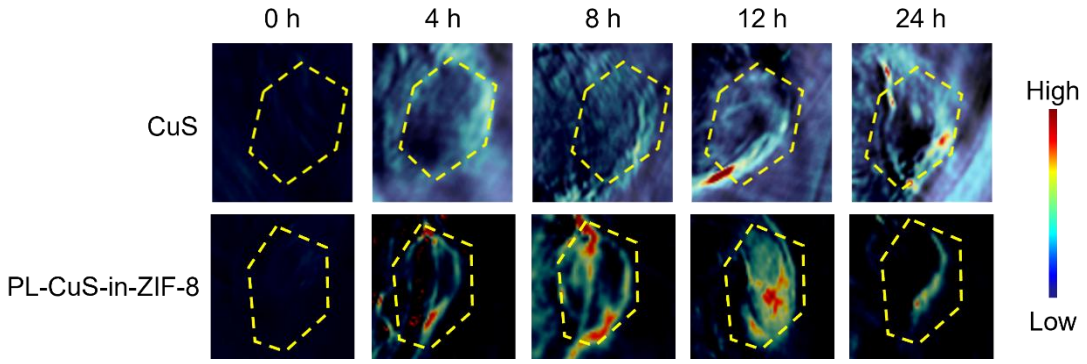

Figure S38. The PAI of tumor at different time points in A549 tumor-bearing mice after being treated with CuS and PL-CuS-in-ZIF-8.

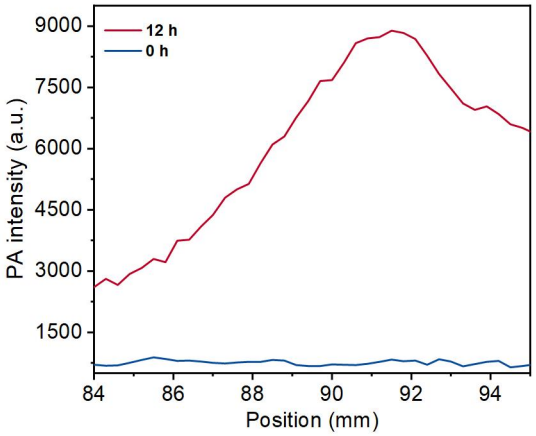

Figure S39. The PA signal intensity in mice injected with PL-CuS-in-ZIF-8 reached its peak 12 h post-injection.

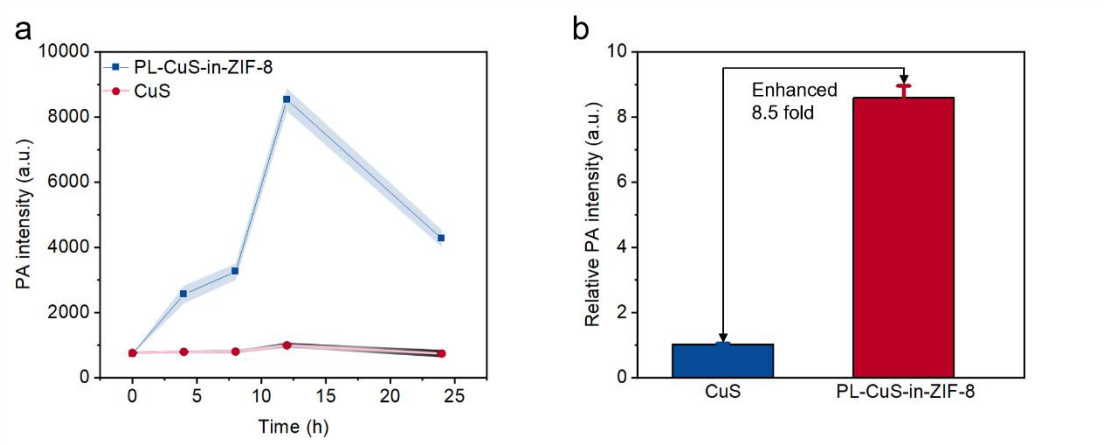

Figure S40. (a) PAI signals intensity at different time points of mice treated with nanoparticles. (b) Quantitative analysis of the PAI signal intensity in mice treated with nanoparticles 12 h post-injection. Data are shown as mean ± SD, n=3.

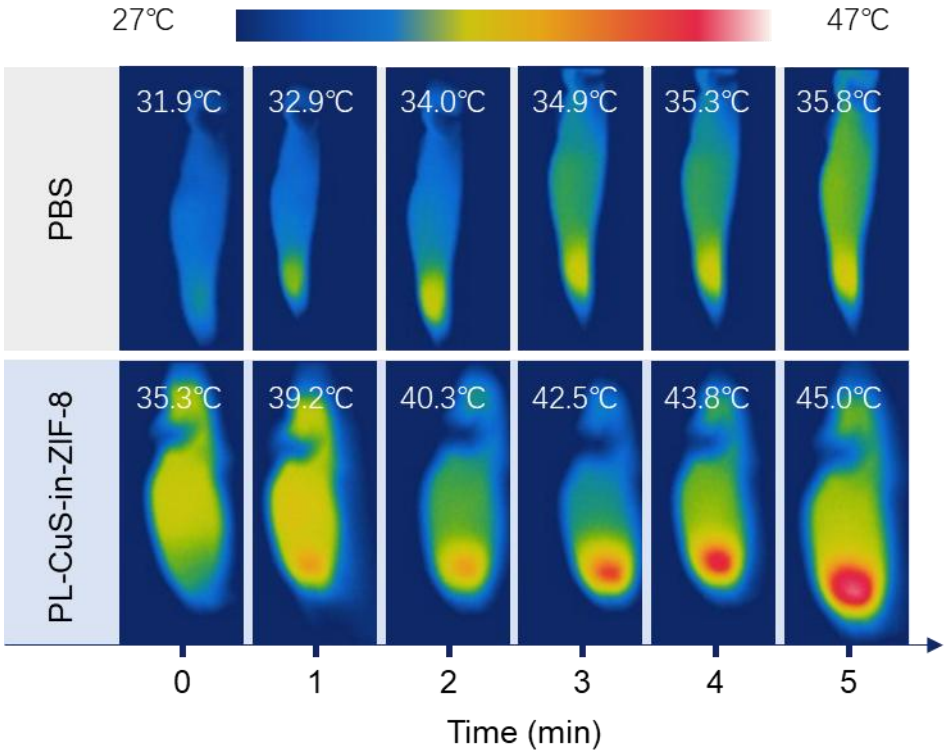

Figure S41. Tumor-bearing mice were injected with PL-CuS-in-ZIF-8 nanoparticles and subjected to irradiation with an 808 nm laser.

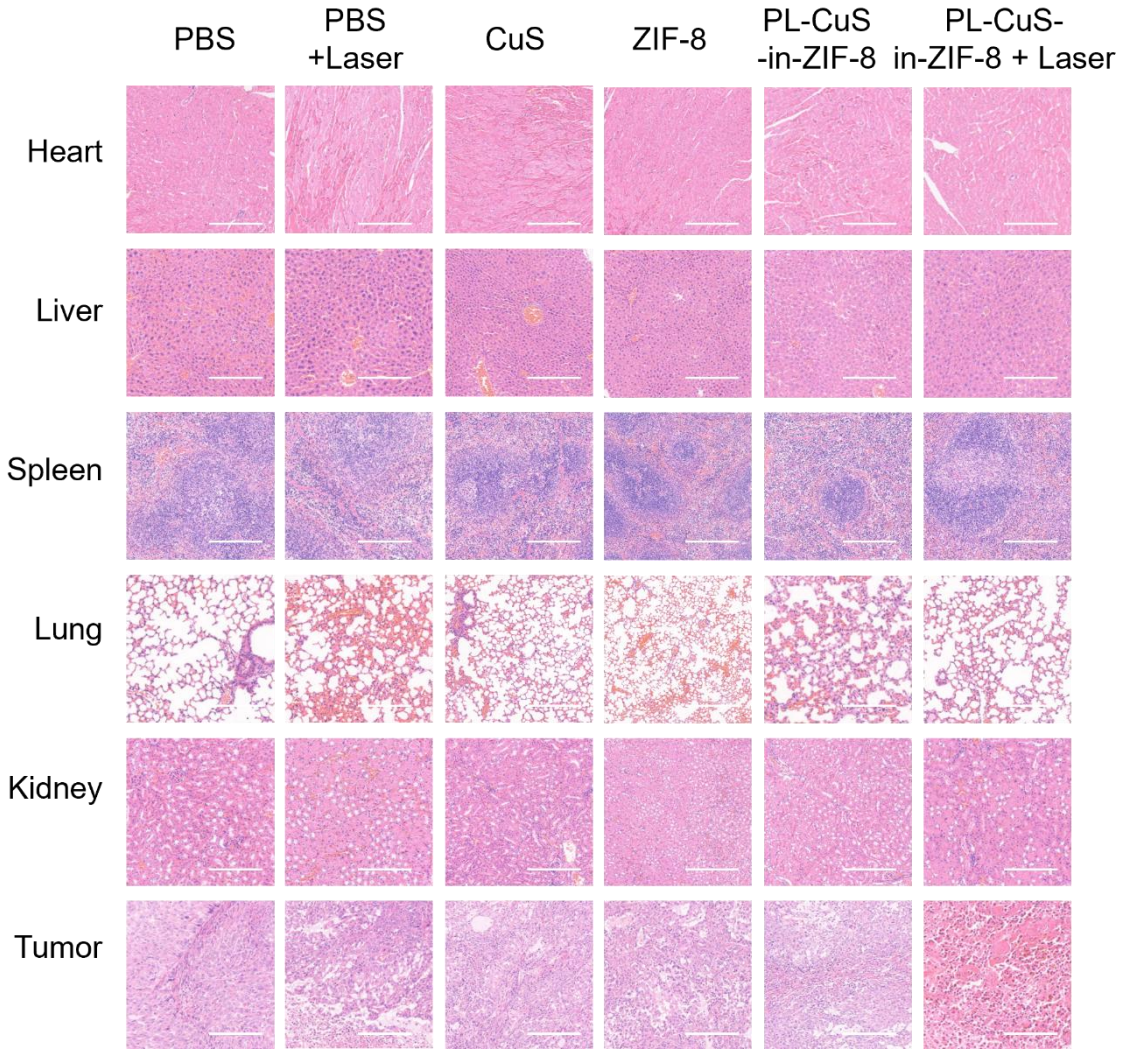

Figure S42. Hematoxylin eosin (H&E) stained images of major organs (Heart, Liver, Spleen, Lung, Kidney, Tumor). The main organs of the mice after injection of 10 mg kg^{-1} PL-CuS-in-ZIF-8 for 16 days. For the light irradiation, (808 nm laser, 5 min, 1 W cm^{-2}) was applied. Scale bar = 200 mm.

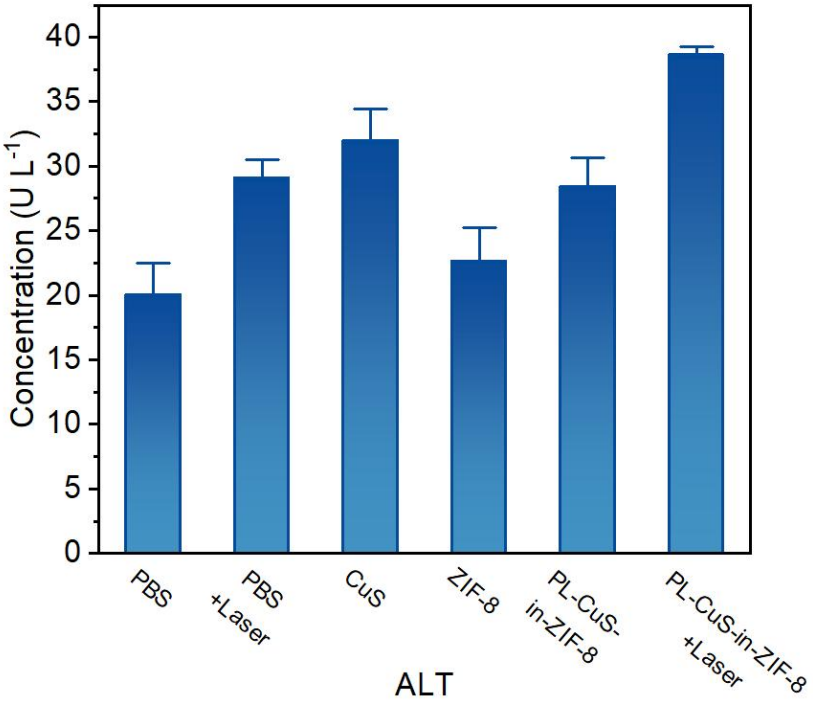

Figure S43. Blood biochemistry of ALT. Data are shown as mean ± SD, n=3.

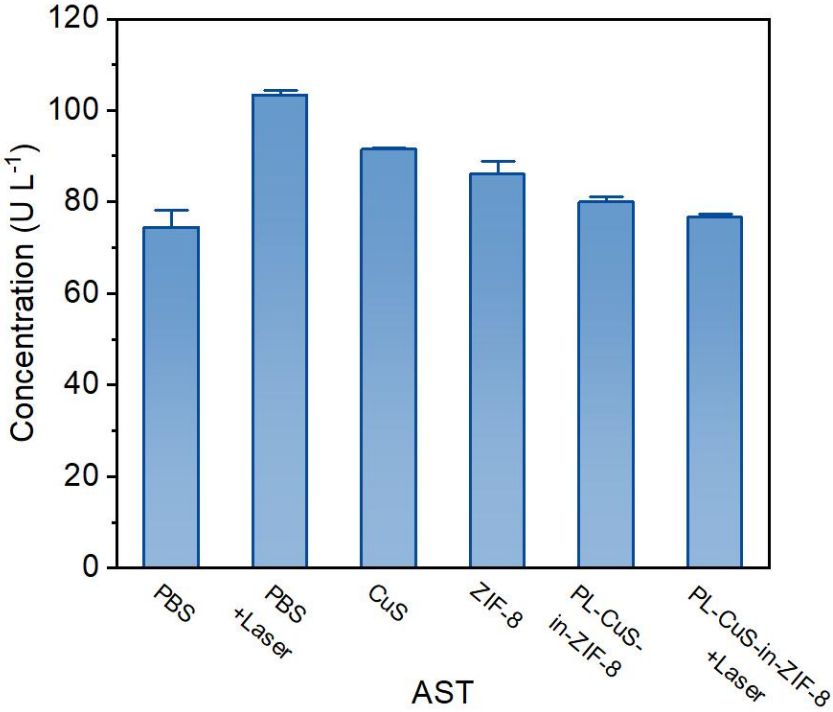

Figure S44. Blood biochemistry of AST. Data are shown as mean ± SD, n=3.

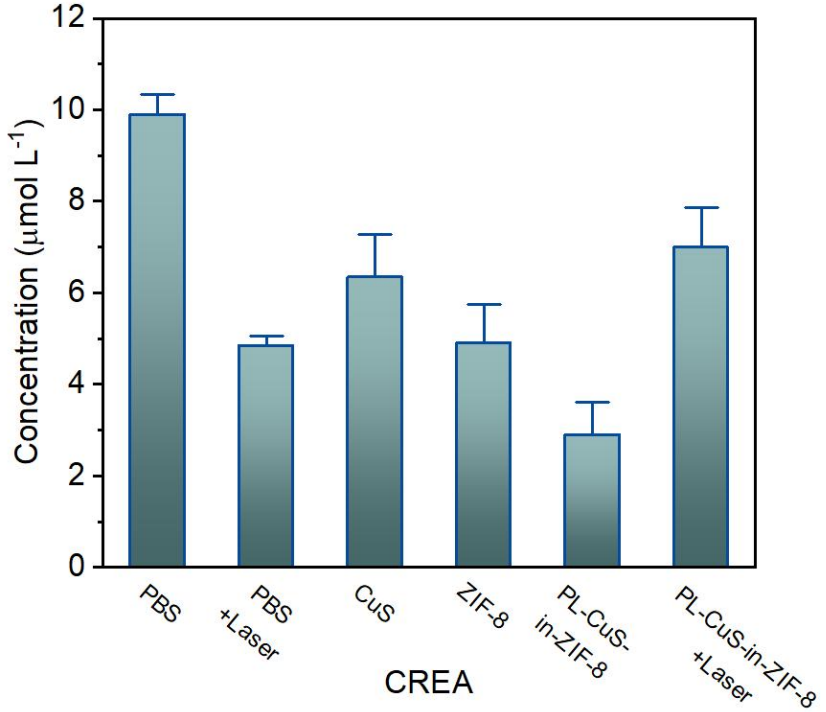

Figure S45. Blood biochemistry of CREA. Data are shown as mean ± SD, n=3.

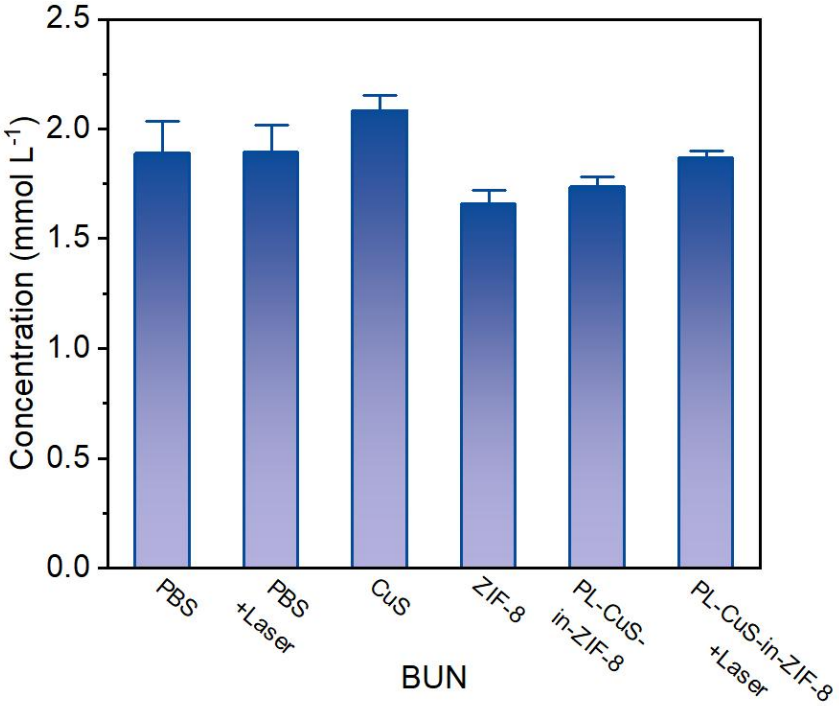

Figure S46. Blood biochemistry of BUN. Data are shown as mean ± SD, n=3.

Table S1. Results of ICP determination of nanoparticles.

Sample	Cu [wt%]	CuS [wt%]	Zn [wt%]
PL-CuS-in-ZIF-8	1.36%	2.04%	24.41%
CL-CuS-in-ZIF-8	1.14%	1.71%	24.29%
SL-CuS-on-ZIF-8	2.13%	3.19%	23.88%

Table S2. Quantified information for ^{129}Xe NMR spectra.

Sample	FWHZ [Hz]	^{129}Xe NMR signal integral
PL-CuS-in-ZIF-8	435.48	331.0
SL-CuS-on-ZIF-8	262.3	160.5
ZIF-8	187.48	357.3
CL-CuS-in-ZIF-8	98.05	213.8

Table S3. Integral values of ^{129}Xe NMR signals before and after laser irradiation.

Laser irradiated	^{129}Xe NMR signal integral
before	101.5
after	106.6

Table S4. Results of ICP-MS determination of nanoparticles with different feeding ratios.

Sample	Cu [wt %]	Zn [wt %]
PL-CuS_{10}-in-ZIF-8	1.79%	25.04%
PL-CuS_{15}-in-ZIF-8	1.36%	24.41%
PL-CuS_{20}-in-ZIF-8	1.76%	24.72%
PL-CuS_{25}-in-ZIF-8	1.67%	23.58%
PL-CuS_{30}-in-ZIF-8	1.78%	24.41%

Table S5. Integral values of ^{129}Xe NMR signals for different PL-CuS-in-ZIF-8 samples.

Sample	^{129}Xe NMR signal integral
PL-CuS_{10}-in-ZIF-8	276.6
PL-CuS_{15}-in-ZIF-8	333.2
PL-CuS_{20}-in-ZIF-8	278.2
PL-CuS_{25}-in-ZIF-8	274.8
PL-CuS_{30}-in-ZIF-8	244.2

Table S6. Integrated values of PL-CuS-in-ZIF-8 ^{129}Xe NMR signals at various concentrations.

Concentration of PL-CuS-in-ZIF-8 [mg mL^{-1}]	^{129}Xe NMR signal integral
2.5	51.5
5.0	106.6
7.5	156.2

10.0	211.2
12.5	218.5

Reference

[1] Z. Wang, X. Tang, X. Wang, D. Yang, C. Yang, Y. Lou, J. Chen, N. He, *Chem. Commun.* **2016**, 52, 12210.